



Glutathione peroxidase 4-regulated neutrophil ferroptosis induces systemic autoimmunity

Pengchong Li^{1,2,7}, Mengdi Jiang^{1,2,7}, Ketian Li^{1,2,7}, Hao Li^{3,7}, Yangzhong Zhou⁴, Xinyue Xiao¹, Yue Xu², Suzanne Krishfield³, Peter E. Lipsky⁵✉, George C. Tsokos³✉ and Xuan Zhang⁶✉

The linkage between neutrophil death and the development of autoimmunity has not been thoroughly explored. Here, we show that neutrophils from either lupus-prone mice or patients with systemic lupus erythematosus (SLE) undergo ferroptosis. Mechanistically, autoantibodies and interferon- α present in the serum induce neutrophil ferroptosis through enhanced binding of the transcriptional repressor CREM α to the glutathione peroxidase 4 (*Gpx4*, the key ferroptosis regulator) promoter, which leads to suppressed expression of *Gpx4* and subsequent elevation of lipid-reactive oxygen species. Moreover, the findings that mice with neutrophil-specific *Gpx4* haploinsufficiency recapitulate key clinical features of human SLE, including autoantibodies, neutropenia, skin lesions and proteinuria, and that the treatment with a specific ferroptosis inhibitor significantly ameliorates disease severity in lupus-prone mice reveal the role of neutrophil ferroptosis in lupus pathogenesis. Together, our data demonstrate that neutrophil ferroptosis is an important driver of neutropenia in SLE and heavily contributes to disease manifestations.

SLE is a chronic debilitating autoimmune disease characterized by a global loss of immune tolerance with activation of both innate and adaptive branches of the immune system¹. Central features include accumulated noncleared cell debris derived from various forms of cell death, elevated type I interferon (IFN) signaling and increased autoantibody production². Neutrophils are the dominant immune cells in the circulation and contribute to a variety of autoimmune disorders. In patients with SLE, a number of abnormalities in neutrophils have been reported, including impaired phagocytosis, increased aggregation and accelerated cell death³. Elevated levels of anti-neutrophil cytoplasmic antibodies in the sera of patients with SLE suggest that neutrophil death together with ineffective clearance of the subsequent debris provides a stable source of autoantigens for disease initiation and propagation⁴. However, the main forms of neutrophil death in SLE and the underlying mechanisms have not been fully characterized.

Ferroptosis is a newly recognized form of programmed cell death that is morphologically, biochemically and genetically distinct from other forms of regulated cell death such as apoptosis, necroptosis and pyroptosis⁵. It is characterized by production of lipid-reactive oxygen species (ROS) and iron overload, leading to caspase- and necrosome-independent cell death. As a key regulator of ferroptosis, phospholipid peroxidase glutathione peroxidase 4 (GPX4) can detoxify hydroperoxides in membrane lipids directly, thereby reducing damage to membrane function and preventing the generation of lipid peroxidation-derived reactive products and mitigating ferroptosis^{6–8}. Inhibition or ablation of GPX4 induces ferroptosis in different cell types^{9–11}. Here, we describe how autoantibodies and type I IFNs cooperatively induce neutrophil ferroptosis in lupus through the calcium/calmodulin

kinase IV (CaMKIV)/CREM α signaling axis. Importantly, the observations that neutrophil-specific *Gpx4* haploinsufficiency in mice gives rise to SLE-like phenotypes and that in vivo inhibition of ferroptosis mitigates disease progression in lupus-prone MRL/*lpr* mice confirm the immunopathogenic effects of neutrophil ferroptosis. Therefore, our results, reported herein, identify a central cellular defect and provide the missing link between neutropenia and lupus pathogenesis.

Results

Serum factors modulate neutrophil viability in SLE. To substantiate the concept that neutropenia is a common feature in SLE, a total of 126 patients with SLE were included in the analysis (Supplementary Tables 1–3). Compared with healthy controls (HCs), neutrophil counts in patients with SLE were significantly reduced, with 35% of them presenting a neutrophil count below $2 \times 10^9 l^{-1}$. In contrast, this was not observed in patients with other autoimmune diseases (Fig. 1a). Moreover, to exclude the potential interference of treatment, 98 patients with newly diagnosed untreated SLE were selected and, as expected, the neutrophil counts correlated inversely with disease activity as measured by the Systemic Lupus Erythematosus Disease Activity Index (SLEDAI) (Fig. 1b). Importantly, the numbers of neutrophils were restored to normal levels after effective treatment with standard-of-care medications (Fig. 1c and Supplementary Table 4).

We next evaluated the viability (live cells were gated as 7AAD⁻Annexin V⁻) of fresh neutrophils isolated from SLE patient blood and, as expected, they displayed lower cell viability compared with those from HCs; notably, effective treatment helped restore neutrophil viability (Fig. 1d). Collectively, these observations led us to

¹State Key Laboratory of Complex Severe and Rare Diseases, Peking Union Medical College Hospital, Chinese Academy of Medical Sciences and Peking Union Medical College, Beijing, China. ²Clinical Immunology Centre, Chinese Academy of Medical Sciences and Peking Union Medical College, Beijing, China. ³Department of Medicine, Beth Israel Deaconess Medical Center, Harvard Medical School, Boston, MA, USA. ⁴Department of Internal Medicine, Peking Union Medical College Hospital, Chinese Academy of Medical Sciences and Peking Union Medical College, Beijing, China. ⁵RILITE Research Institute and AMPEL BioSolutions, Charlottesville, VA, USA. ⁶Department of Rheumatology, Beijing Hospital, National Center of Gerontology, Institute of Geriatric Medicine, Chinese Academy of Medical Sciences, Beijing, China. ⁷These authors contributed equally: Pengchong Li, Mengdi Jiang, Ketian Li, Hao Li. ✉e-mail: peterlipsky@comcast.net; gsokos@bidmc.harvard.edu; zxpmch2003@sina.com

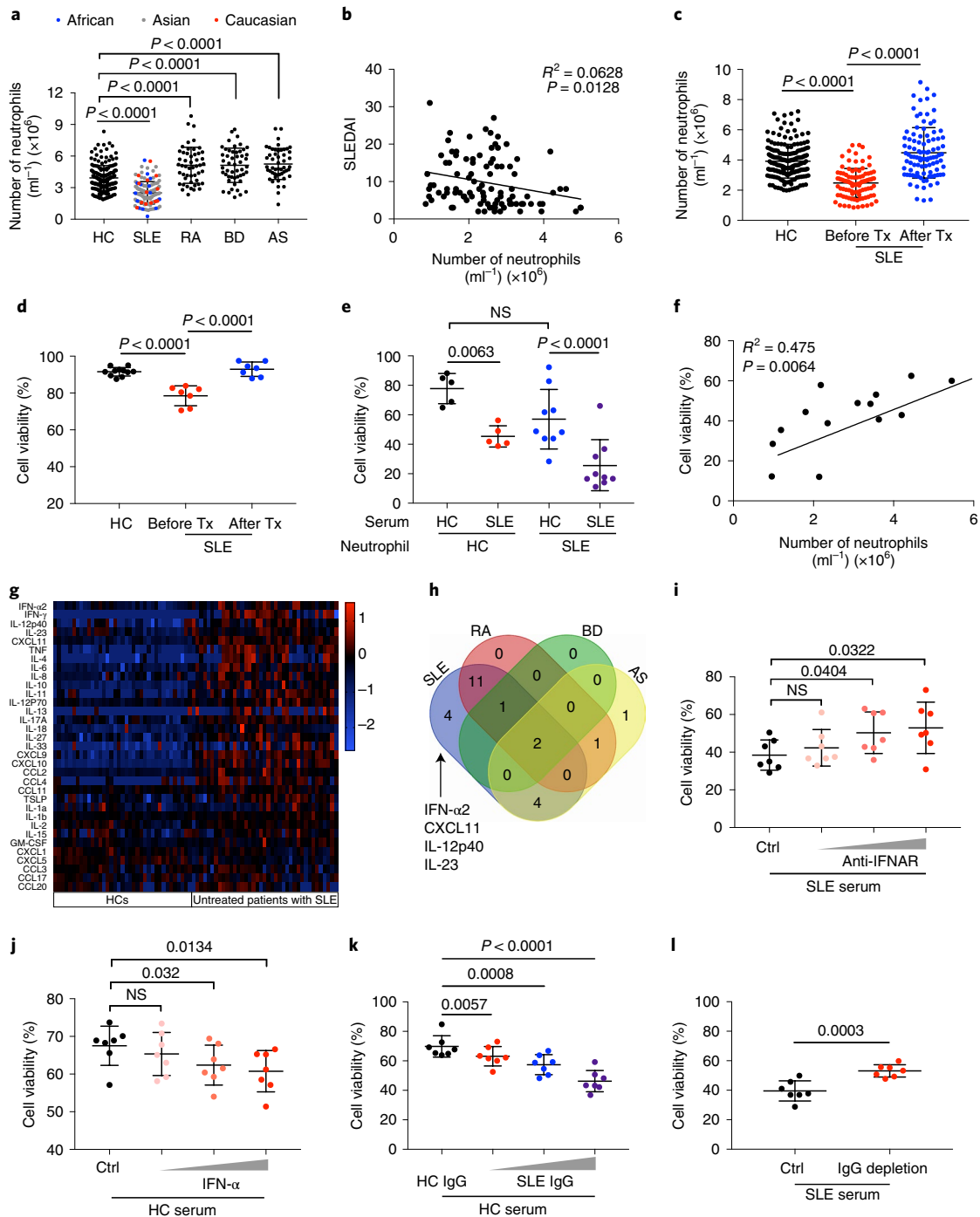


Fig. 1 | SLE IgG and IFN- α modulate neutrophil viability. **a**, The numbers of peripheral neutrophils from either HCs or patients with different rheumatic diseases including SLE, RA, Behcet's disease (BD) and ankylosing spondylitis (AS) (HC: $n = 188$; SLE: $n = 126$; RA: $n = 50$; BD: $n = 50$; AS: $n = 50$). **b**, The numbers of peripheral neutrophils in SLE correlated negatively with disease activity as measured by the SLEDAI ($n = 98$). **c**, The numbers of peripheral neutrophils in patients with SLE ($n = 98$) before and after treatments versus HCs. **d**, Flow cytometry quantification of cell viability of neutrophils freshly isolated from peripheral blood of patients with SLE before and after treatment ($n = 7$) versus HCs ($n = 11$) (live cells were defined as 7AAD⁻AnexinV⁻). **e**, Flow cytometry quantification of cell viability of neutrophils cultured in vitro with 20% serum from either HCs ($n = 5$) or patients with SLE ($n = 9$) for 16 h. **f**, The in vitro effect of SLE sera on neutrophil cell viability correlated with the peripheral neutrophil counts in patients with SLE ($n = 14$). **g**, Multiplex cytokine array of the inflammatory factors present in sera from patients with SLE versus HCs (SLE = 39, HC = 37). **h**, Venn diagram showing serum factors specifically increased in SLE. **i, j**, Flow cytometry quantification of cell viability of neutrophils ($n = 7$) cultured in vitro with SLE serum supplemented with blocking antibody targeting IFN- α at different dosages (0.1, 1, 10 $\mu\text{g ml}^{-1}$) (**i**), or with HC serum with the addition of IFN- α at different dosages (10³, 10⁴, 10⁵ U ml⁻¹) (**j**) for 16 h. **k, l**, Flow cytometry quantification of cell viability of neutrophils ($n = 7$) from HCs cultured with HC serum with the addition of SLE IgG at different dosages (1.2, 2.4, 3.6 g l^{-1}) (**k**), or SLE serum with/without IgG depletion (**l**), for 16 h. Data are shown as mean \pm s.d. Not significant (NS) $P > 0.05$. Two-tailed unpaired or paired Student's t -test was applied. Ctrl, control; Tx, treatment.

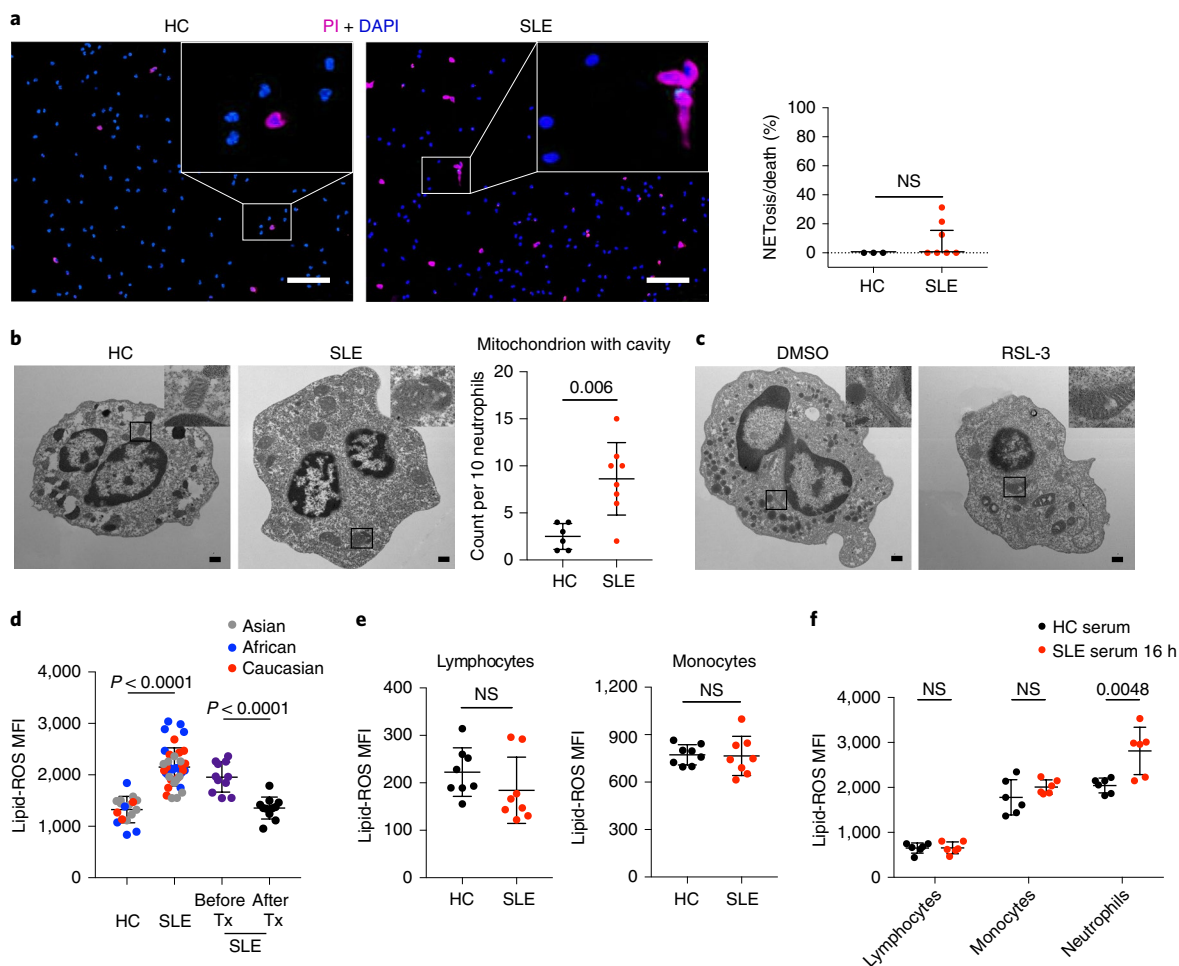


Fig. 2 | Neutrophil ferroptosis is prevalent in patients with SLE. **a**, Left, representative fluorescent images indicate neutrophil death. Peripheral neutrophils from both HCs and patients with SLE were stained with PI to detect dead cells and with DAPI as counterstain, and NETs were defined as cells with DNA area exceeding $400 \mu\text{m}^2$. The scale bar represents $100 \mu\text{m}$. Right, dot plots show the quantification (HC: $n=3$; SLE: $n=7$). **b**, Left, representative electron microscopy images of neutrophils in HCs and patients with SLE. Right, quantification of neutrophil mitochondria with cavities in HCs ($n=6$) and patients with SLE ($n=8$). The scale bar represents 500nm . **c**, Representative electron microscopy images of HC neutrophils cultured with 20% HC serum supplemented with dimethylsulfoxide vehicle or $10 \mu\text{M}$ RSL-3, a ferroptosis inducer, for 4 h. The scale bar represents 500nm . **d**, Lipid-ROS content in neutrophils from patients with SLE ($n=39$); paired SLE samples before and after treatment ($n=11$); neutrophils from HCs were used as controls ($n=17$). Cells were incubated with BODIPY C11, a fluorescent lipid peroxidation reporter molecule that shifts its fluorescence from red to green, for 15 min before flow cytometry assessment. **e**, Flow analysis of lipid-ROS content in lymphocytes and monocytes from either HCs or patients with SLE ($n=8$). **f**, Flow analysis of lipid-ROS content in HC lymphocytes, monocytes and neutrophils after being cultured with 20% HC or SLE serum, respectively, for 16 h ($n=6$). Data are shown as mean \pm s.d. or median with interquartile range. NS, $P > 0.05$. Two-tailed unpaired or paired Student's *t*-test or Mann-Whitney test was applied. DMSO, dimethylsulfoxide; MFI, mean fluorescence intensity.

hypothesize that the sera from patients with active SLE may promote neutrophil death. As expected, neutrophils cultured with SLE sera displayed significantly reduced viability (Fig. 1e and Extended Data Fig. 1a) and this reduction correlated positively with the severity of neutropenia in the patients (Fig. 1f and Supplementary Table 5). Of note, serum from patients with rheumatoid arthritis (RA) did not have the same effect (Extended Data Fig. 1b). To determine key factors in SLE sera responsible for this effect, we compared cytokine profiles in SLE sera with those in other autoimmune diseases and HCs. Four cytokines were specifically increased in SLE, namely IFN- α , chemokine C-X-C motif ligand 11 (CXCL11), interleukin-12p40 (IL-12p40) and IL-23 (Fig. 1g,h and Extended Data Fig. 1c). However, blockade of type I IFN signaling, but not of the other cytokines¹², abrogated the enhanced neutrophil death mediated by SLE sera (Fig. 1i and Extended Data Fig. 1d), and the addition of IFN- α to HC serum promoted neutrophil death (Fig. 1j).

These results indicate that type I IFN contributes to neutrophil death in patients with lupus.

The production of autoantibodies is a hallmark of SLE and plays a critical role in disease pathogenesis^{13,14}. Interestingly, the proportion of autoantibodies, such as anti-dsDNA IgG, in total IgG correlated positively with the severity of neutropenia (Extended Data Fig. 1f,g). To investigate whether autoantibodies are involved in neutrophil death, we purified total IgG from either healthy or SLE sera (Extended Data Fig. 1h,j), and applied them to healthy neutrophils in the presence of HC serum. As expected, SLE but not healthy IgG reduced the viability of neutrophils in a concentration-dependent manner (Fig. 1k and Extended Data Fig. 1k). Consistently, the depletion of IgG from SLE serum reduced the ability of serum to decrease cell viability of cultured neutrophils and the addition of IFNAR-neutralizing antibody further curtailed this modulating capability (Fig. 1l and Extended Data Fig. 1l,k). Taken together,

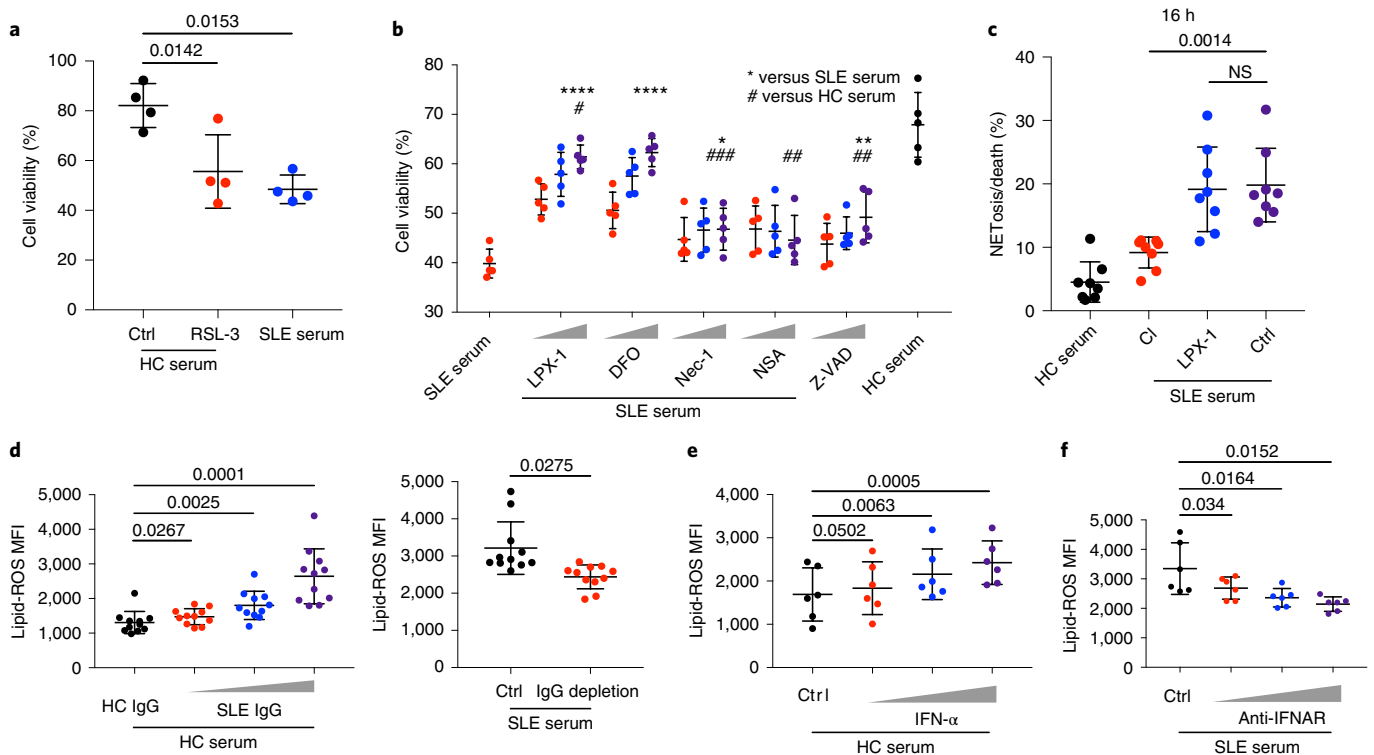


Fig. 3 | Neutrophil ferroptosis, the main form of neutrophil death in SLE, is induced by autoantibodies and IFN- α . **a**, HC neutrophil cell viability when cultured with 20% HC serum supplemented with RSL-3 (10 μ M) or dimethylsulfoxide for 16 h; cell viabilities were assessed by flow cytometry ($n=4$). **b**, HC neutrophil cell viability when cultured in 20% HC or SLE serum supplemented with increasing dosages of various reagents, including two ferroptosis inhibitors, LPX-1 (10/100/1,000 nM) or DFO (1/10/100 μ M); two necroptosis inhibitors, Nec-1 (10/100/1,000 nM) or NSA (10/100/1,000 nM); or apoptosis inhibitor Z-VAD (0.1/1/10 μ M) for 16 h; cell viabilities were assessed by flow cytometry ($n=5$). **c**, HC neutrophils were cultured in the presence of HC or SLE serum with or without addition of Cl-amidine (Cl) (an inhibitor of NETosis, 100 μ M) or LPX-1 (1 μ M) for 16 h, and NETs were counted in SYTOX Green⁺ cells by morphology ($n=8$). Neutrophils with DNA area greater than 400 μ m² were considered to have undergone NETosis. Dot plots show the percentage of NETosis in all dead neutrophils in the indicated group. **d**, Lipid-ROS production by HC neutrophils when cultured with 20% HC serum supplemented with SLE IgG, or with SLE serum with or without IgG depletion, for 16 h ($n=11$). **e**, Lipid-ROS production by HC neutrophils when stimulated with IFN- α at different concentrations (10³, 10⁴, 10⁵ U ml⁻¹) for 16 h ($n=6$). **f**, Lipid-ROS production by HC neutrophils when cultured with SLE serum in the absence or presence of IFNAR blocking antibody at different dosages (0.1, 1, 10 μ g ml⁻¹) for 16 h ($n=6$). Data are shown as mean \pm s.d. * or # $P < 0.05$, ** or ## $P < 0.01$, *** or ### $P < 0.001$, **** $P < 0.0001$; NS, $P > 0.05$. Two-tailed unpaired or paired Student's t -test was applied.

these results suggest that SLE IgG and IFN- α present in SLE sera induce neutrophil death.

Neutrophil ferroptosis is prevalent in patients with SLE. NETosis, a unique form of neutrophil death characterized by the release of decondensed chromatin and granular contents to the extracellular space, has been proposed as an important cause of neutropenia in lupus¹⁵. To test this, peripheral neutrophils from both HCs and patients with SLE were stained with propidium iodide (PI) to detect dead cells and DAPI as counterstain, and neutrophil extracellular traps (NETs) were defined as cells with a surrounding DNA area exceeding 400 μ m² (ref. 16). We observed only a small portion of dead neutrophils that could be attributed to NETosis (Fig. 2a). Therefore, we further looked into neutrophil death by electron microscopy, and we found that a significant portion of neutrophils isolated from patients with SLE exhibited typical morphological characteristics of ferroptosis⁵, including mitochondrial vacuole formation with increased mitochondrial membrane density and disappearance of mitochondrial cristae (Fig. 2b). Similar morphologic changes were recapitulated in HC neutrophils treated with RSL-3, a ferroptosis inducer¹⁷ (Fig. 2c). Consistent with this, the levels of lipid-ROS, both an indicator and a strong inducer of ferroptosis⁵, were higher in patients with SLE with active diseases

but were remarkably reduced after effective systemic treatment (Fig. 2d). Of note, the increased levels of lipid-ROS were restricted to neutrophils and did not extend to lymphocytes or monocytes from patients with SLE, and consistently SLE serum induced lipid-ROS and reduced cell viability in neutrophils only (Fig. 2e,f and Extended Data Fig. 2a,b). In contrast to the finding that RSL-3 induced death in neutrophils cultured with HC serum, two ferroptosis inhibitors, liproxstatin-1 (LPX-1) and the iron chelator deferoxamine (DFO), rescued neutrophil death induced by SLE serum^{5,18} (Fig. 3a,b and Extended Data Fig. 2c–e), suggesting that ferroptosis may be the main form of neutrophil death in SLE. Of note, LPX-1 did not inhibit NETosis and had no or negligible effect on B cell or plasmacytoid dendritic cell (pDC) function, indicated by antibody or type I IFN production, respectively (Fig. 3c and Extended Data Figs. 2f,g and 3a–e). Notably, necroptosis inhibitors, necrosulfonamide (NSA) and necrostatin-1 (Nec-1), and the apoptosis inhibitor, Z-VAD, produced only minimal effects on neutrophil death (Fig. 3b). It has been shown that direct inhibition of GSH synthesis induces ferroptosis¹⁹. Of note, low dose of β -ME could partially rescue neutrophil death by boosting GSH biosynthesis (Extended Data Fig. 2h,i). Collectively, these findings indicate that ferroptosis is the main driver of neutrophil death in patients with SLE.

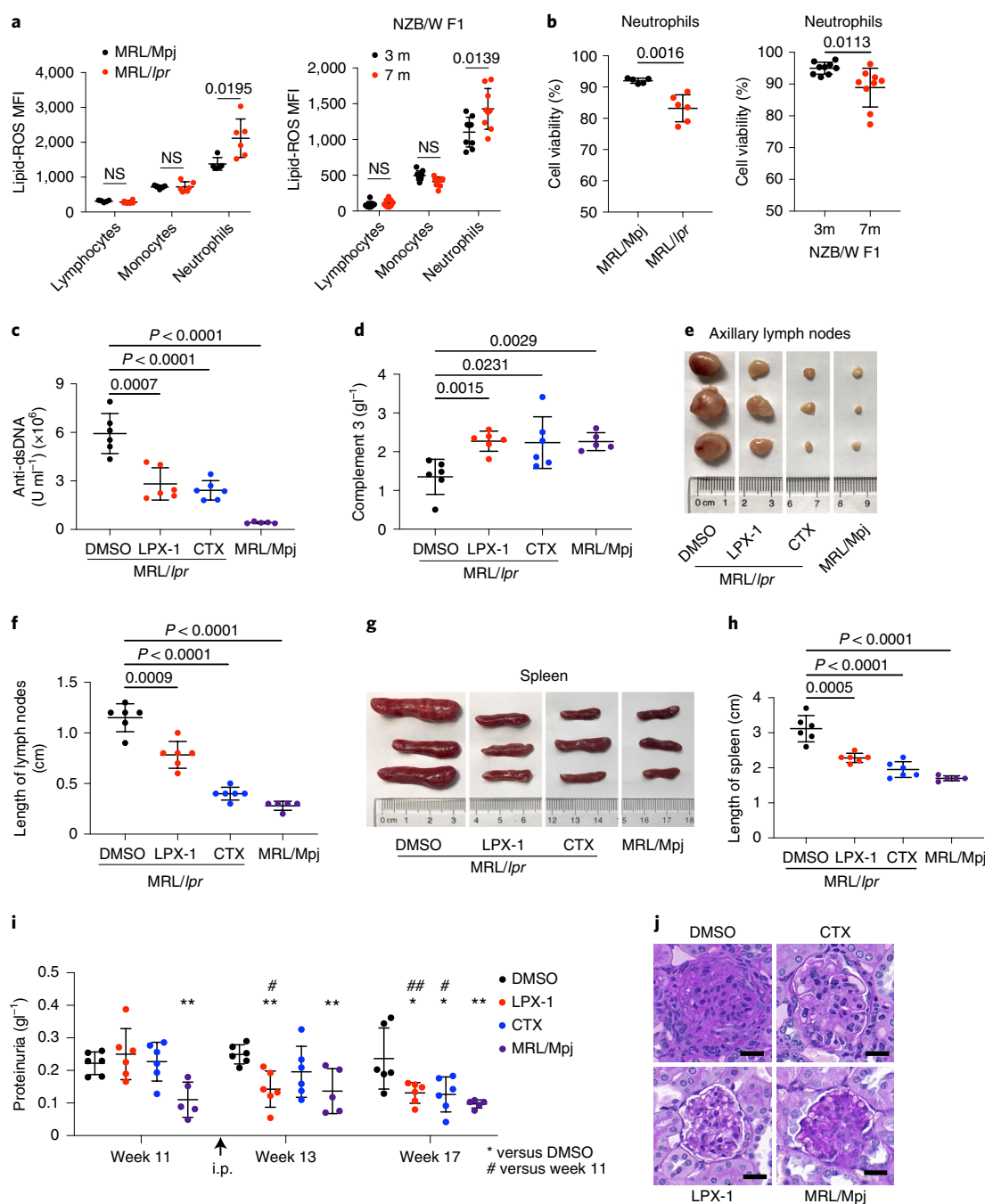


Fig. 4 | Ferroptosis inhibitors ameliorate disease progression in MRL/lpr mice. **a**, Flow cytometry quantification of lipid-ROS in lymphocytes, monocytes and neutrophils from MRL/Mpj ($n=6$), MRL/lpr ($n=6$) and NZB/W F1 mice ($n=9$). Splenic cells were incubated with BODIPY C11 for 15 min before flow cytometry assessment. **b**, Cell viability of circulating neutrophils from indicated mice was quantified by flow cytometry (MRL/Mpj and MRL/lpr were euthanized at 18 weeks of age for analysis, NZB/W F1 at 3 or 7 months of age). **c–j**, MRL/lpr mice ($n=6$) were treated with dimethylsulfoxide, LPX-1 or CTX every other day for 6 weeks starting at week 12; dimethylsulfoxide was applied to sex-matched MRL/Mpj mice ($n=5$) as control. Mice were euthanized at 18 weeks of age for analysis. **c**, ELISA assessment of serum anti-dsDNA titers. **d**, ELISA assessment of serum complement 3. **e, f**, Representative images (**e**) and length quantification (**f**) of axillary lymph nodes. **g, h**, Representative images (**g**) and length (**h**) of spleens. **i**, Bicinchoninic acid (BCA) assay of urine proteins. **j**, Periodic acid-Schiff staining of glomeruli. The scale bar represents 20 μm . Data are shown as mean \pm s.d. * or # $P < 0.05$, ** or ## $P < 0.01$; NS, $P > 0.05$. Two-tailed unpaired Student's t -test was applied. i.p., intraperitoneal injection; m, month.

As was expected, the addition of SLE IgG or IFN- α to HC serum increased neutrophil lipid-ROS in a concentration-dependent manner (Fig. 3d,e), whereas IgG depletion or treatment with IFNAR-neutralizing antibodies reduced the capacity of SLE sera to induce lipid-ROS production by neutrophils (Fig. 3d,f and Extended Data Fig. 1e). Although both IFN- α and SLE IgG induced neutrophil

ferroptosis, SLE IgG was a more potent inducer. Of note, although there was approximately 20% NETosis in total dead neutrophils induced by IFN- α stimulation alone, the addition of SLE IgG clearly re-programmed the neutrophil death program indicated by a significant decrease of NETosis in the face of slightly enhanced neutrophil death (Extended Data Fig. 3f–i). Taken together, our results suggest

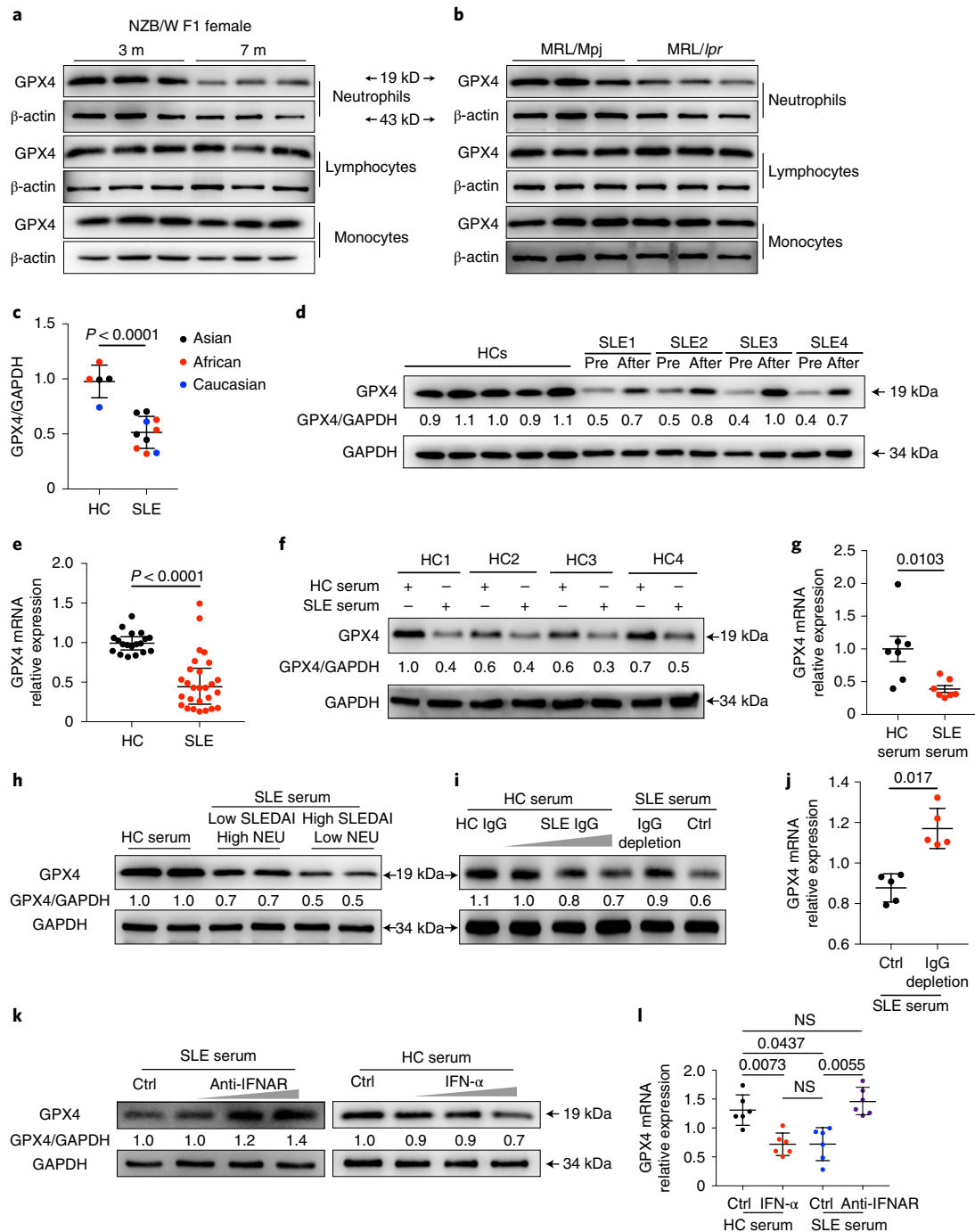


Fig. 5 | IFN- α and SLE IgG are the main drivers of neutropenia by reducing GPX4 in neutrophils. **a,b**, Western blot analysis of GPX4 expression in lymphocytes, monocytes and neutrophils from NZB/W F1 (**a**) and MRL/Mpj and MRL/lpr (**b**) mice. **c–e**, Western blot (HC = 5, SLE = 10) (**c**) and qPCR analysis (HC = 19, SLE = 27) (**e**) of GPX4 expression in neutrophils isolated from HCs and patients with SLE. Paired SLE samples before and after effective treatments were analyzed (**d**). **f,g**, Western blot (**f**) and qPCR (**g**) analysis of GPX4 expression in HC neutrophils cultured with 20% HC or SLE serum for 30 h ($n = 7$). **h**, Western blot analysis of GPX4 expression in HC neutrophils cultured for 30 h with 20% HC or SLE serum with different disease activities and neutrophil (NEU) counts. **i,j**, Western blot (**i**) and qPCR (**j**) analysis of GPX4 expression in HC neutrophils when cultured with HC serum supplemented with SLE IgG (1.2, 2.4, 3.6 $\mu\text{g l}^{-1}$), or with SLE serum with or without IgG depletion, for 16 h ($n = 5$). **k,l**, Western blot (**k**) and qPCR (**l**) analysis of GPX4 expression in HC neutrophils when cultured with HC serum supplemented with IFN- α (10^3 , 10^4 , 10^5 U ml^{-1}) or SLE serum supplemented with anti-IFNAR monoclonal antibody (0.1, 1, 10 $\mu\text{g ml}^{-1}$) ($n = 6$). Data are shown as mean \pm s.d. NS, $P > 0.05$. Two-tailed unpaired or paired Student's *t*-test was applied.

that in the SLE milieu, neutrophil ferroptosis is a dominant form of neutrophil death considering the co-presence of IFN- α and IgG.

Inhibition of ferroptosis attenuates lupus in mice. We next examined neutrophil ferroptosis in different lupus-prone mice^{20,21}.

Consistent with our finding in patients with SLE, we observed decreased neutrophil viability and increased lipid-ROS production in both MRL/lpr and NZB/W F1 mice (Fig. 4a,b). Furthermore, LPX-1 treatment of MRL/lpr mice at 12 weeks of age efficiently inhibited the production of lipid-ROS in neutrophils, significantly

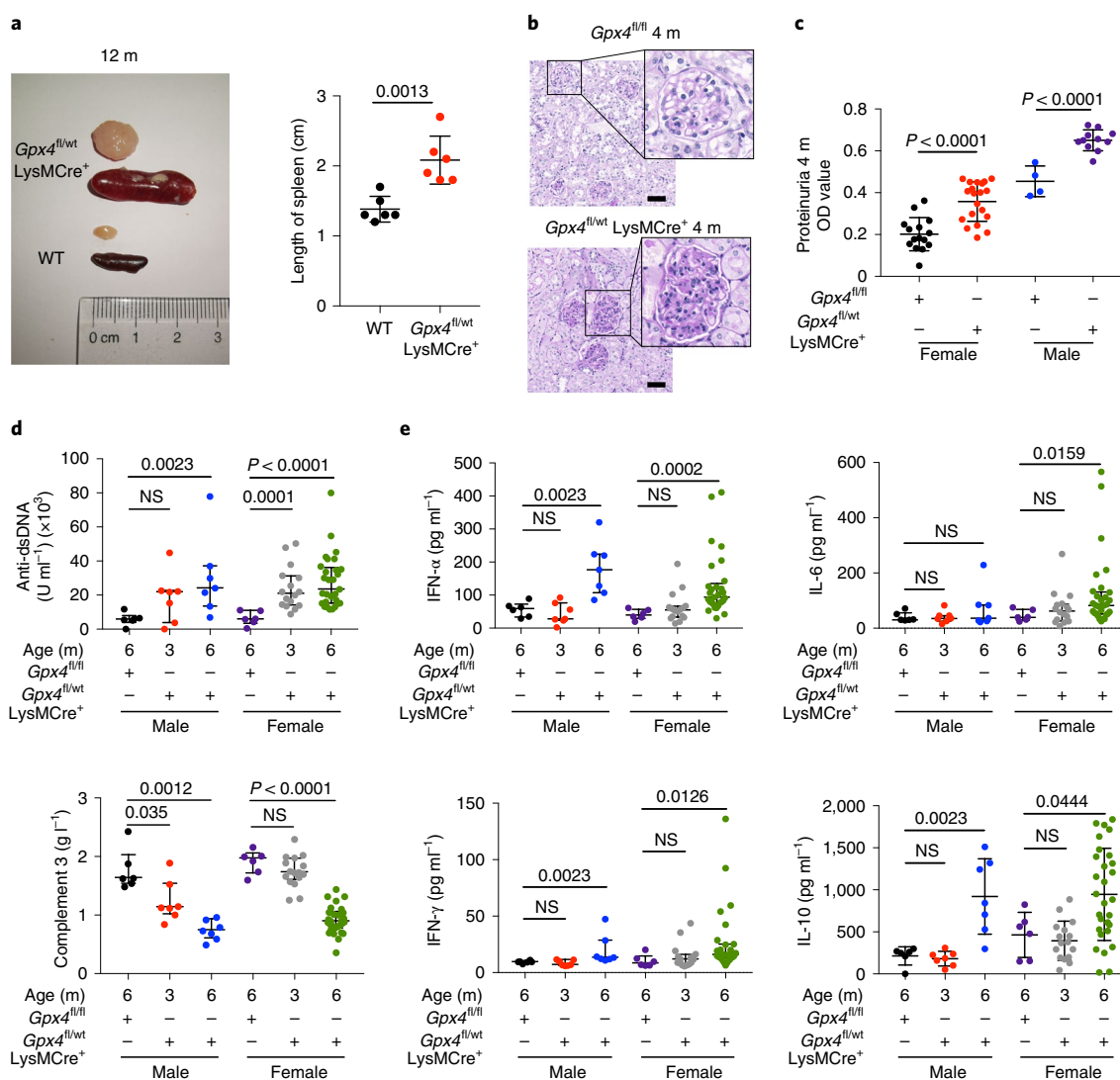


Fig. 6 | Mice with Gpx4 haploinsufficiency in neutrophils develop spontaneous lupus-like disease. a, Size and length of spleen and lymph node from Gpx4^{fl/wt}LysMCre⁺ and wild-type (WT) mice at 12 months of age ($n=6$). **b**, Glomeruli of WT and Gpx4^{fl/wt}LysMCre⁺ mice at 4 months of age (periodic acid-Schiff staining). The scale bar represents 50 μm . **c**, Proteinuria of Gpx4^{fl/fl} and Gpx4^{fl/wt}LysMCre⁺ mice at 4 months of age (BCA assay) (Gpx4^{fl/fl}: female = 15, male = 4; Gpx4^{fl/wt}: female = 20, male = 11). **d, e**, The titers of circulating anti-dsDNA, complement 3 (**d**) and various inflammatory factors (**e**) in Gpx4^{fl/fl} and Gpx4^{fl/wt}LysMCre⁺ mice at different ages by ELISA and Multiplex cytokine detection (Gpx4^{fl/fl}: female = 6, male = 6; Gpx4^{fl/wt}LysMCre⁺: female (3 m/6 m) = 16/29, male (3 m/6 m) = 7/7). Data are shown as mean \pm s.d. or median with interquartile range. NS, $P > 0.05$. Two-tailed unpaired or paired Student's t -test or Mann-Whitney test was applied. OD, optical density.

mitigated disease progression, and reduced the production of auto-antibodies and various inflammatory cytokines, as well as increased serum complement component 3 (C3), and limited splenomegaly, lymphadenopathy and severity of lupus nephritis (Fig. 4c–j and Extended Data Fig. 4a–i). Cytoxin (CTX), a drug used to treat people with SLE, was administered as control²². Of note, the NETosis inhibitor Cl-amidine did not provide equivalent therapeutic values as LPX-1, confirming the distinct role of neutrophil ferroptosis in lupus pathogenesis (Extended Data Fig. 4j–o). Taken together, these results suggest that neutrophil ferroptosis is a main cause of neutropenia in lupus and that targeted therapies and correction of this abnormality yield therapeutic effects.

SLE IgG and IFN- α suppress GPX4 expression in neutrophils.

We next conducted RNA-sequencing (RNA-seq) analysis and compared neutrophil ferroptosis-related gene expression between HCs and patients with SLE, and identified 21 down-regulated genes and

two upregulated genes in SLE neutrophils (Extended Data Fig. 5a and Supplementary Tables 6 and 7). Given that GPX4 has been reported to be a key negative regulator of ferroptotic cell death by removing lipid peroxides^{6,23,24}, we confirmed that GPX4 expression was significantly decreased in the neutrophils but not other immune cells from both lupus-prone mice and people with SLE (Fig. 5a–e, Extended Data Fig. 6a–e and Supplementary Table 5), although the expression of SLC7A11 was not significantly changed (Extended Data Fig. 5b,c). The expression of GPX4 in neutrophils correlated inversely with SLEDAI score but was restored to normal levels after effective systemic treatment (Fig. 5d, Extended Data Fig. 6b and Supplementary Table 5). Furthermore, when we examined GPX4 expression in neutrophils cultured with different sera, we found, not surprisingly, that GPX4 expression was down-regulated when cultured with SLE serum, especially from patients with active disease and neutropenia, but not HC serum (Fig. 5f–h and Extended Data Fig. 6h,i).

As autoantibodies and type I IFNs were found to be pivotal in inducing neutrophil ferroptosis, we next examined their effect on GPX4 expression in neutrophils. As expected, we observed that autoantibodies and IFN- α suppressed the expression of GPX4, whereas addition of anti-IFNAR or IgG depletion reduced the ability of SLE serum to downregulate GPX4 (Fig. 5i–l). Of note, in healthy donors, neutrophils express significantly lower GPX4 compared with other immune cells, which may explain why neutrophils are more sensitive to SLE serum-induced ferroptosis considering their much lower threshold of ferroptosis induction (Extended Data Fig. 6f,g). Of note, GPX4 expression was not affected by NETosis inhibitors (Extended Data Fig. 6j,k). The expression correlation analysis indicated the involvement of Fc γ R3 β in neutrophil ferroptosis by regulating GPX4 (Extended Data Fig. 7a,b). The high expression of Fc γ R3 β in neutrophils aligned with the finding that the overexpression of Fc γ R3 β significantly enhanced the sensitivity of HL60 cells to SLE IgG-induced GPX4 reduction, confirming the role of Fc γ R3 β in SLE IgG-mediated neutrophil ferroptosis (Extended Data Fig. 7c–e). Because Toll-like receptor (TLR)-dependent mechanisms have been shown to trigger NETosis^{3,25}, more information is needed to exclude their relevant contribution to neutrophil ferroptosis. Together, our results demonstrate that the autoantibodies and the increased IFN- α in SLE sera downregulate the expression of GPX4 and lead to neutrophil ferroptosis.

***Gpx4*^{fl/wt} LysMCr⁺ mice develop lupus-like disease.** To validate the pathogenic role of neutrophil ferroptosis in vivo, we generated a myeloid-cell-specific *Gpx4* haploinsufficient mouse (*Gpx4*^{fl/wt} LysMCr⁺) to examine the direct contribution of defective GPX4 expression in neutrophils to the breakdown of immune tolerance. As expected, *Gpx4*^{fl/wt} LysMCr⁺ mice showed reduction of GPX4 expression in neutrophils (Extended Data Fig. 8a,b). Of note, the percentage and absolute cell count of neutrophils in the peripheral blood were significantly decreased in *Gpx4*^{fl/wt} LysMCr⁺ mice, which mimicked the neutropenia in patients with SLE (Extended Data Fig. 8c,d). The increased lipid-ROS production and decreased neutrophil viability in these mice phenocopied what we noted in patients with SLE, and also these defects could be rescued by addition of LPX-1 (Extended Data Fig. 8e). Furthermore, we observed lupus-like manifestations, including the production of inflammatory cytokines and autoantibodies, development of skin lesions, splenomegaly, lymphadenopathy, proteinuria and glomerular deposition of IgG, IgM and C1q in *Gpx4*^{fl/wt} LysMCr⁺ mice (Fig. 6a–e and Extended Data Fig. 8f,g). Interestingly, *Gpx4*^{fl/wt} LysMCr⁺ mice with homozygous GPX4 reduction exhibited only mild signs of autoimmunity with extremely low neutrophils in vivo, which was consistent with the fact that neutrophils are requisite in lupus pathogenesis (Extended Data Fig. 8h–j). Collectively, the *Gpx4*^{fl/wt} LysMCr⁺ mice represent a mouse model to study lupus and the findings herein strongly support the role of neutrophil ferroptosis in the immunopathogenesis in SLE.

SLE IgG and IFN- α promote CREM α binding to the *Gpx4* promoter. Next, we aimed to explore the molecular pathway regulating ferroptosis in neutrophils. By nucleotide sequence analysis, we found a conserved cAMP response element (CRE) located at 42~35 base pairs upstream of the human *Gpx4* promoter, which was a critical binding site for cAMP response element-binding protein (CREB) and cAMP response element modulator (CREM)^{26,27}. CREM α is a widely expressed transcriptional repressor that has been implicated in the termination of T cell immune responses, and increased CREM α in SLE T cells has been linked to decreased IL-2 and increased IL-17F production^{28,29}. CaMKIV has been demonstrated to be involved in the translocation of CREM α to the nucleus and its binding to the CRE sites³⁰. As expected, we observed increased nuclear accumulation of both CaMKIV and CREM α in SLE neutrophils (Fig. 7a and Extended Data Fig. 9a). This phenomenon could also be induced in HC neutrophils by culture with SLE serum, or with HC serum supplemented with either SLE IgG or IFN- α (Fig. 7b,c). In contrast, SLE serum with either depletion of IgG or addition of IFNAR-neutralizing antibodies failed to induce nuclear translocation of these two molecules (Fig. 7b,c). These data indicate that autoantibodies and type I IFNs induce nuclear translocation of both CaMKIV and CREM α in SLE neutrophils.

In agreement with the increased CREM α nuclear accumulation, the enhanced binding of CREM α to the site 42 base pair upstream of *Gpx4* promoter was observed in SLE neutrophils (Fig. 7d). In addition, enrichment of CREM α correlated positively with the activation of type I IFN signaling (Fig. 7e). Moreover, SLE neutrophils displayed increased binding of nuclear CREM α to the site 42 base pair upstream of the *Gpx4* promoter as assessed by DNA pull-down assay (Fig. 7f). Accordingly, the binding of CREM α to the *Gpx4* promoter was increased in HC neutrophils cultured with SLE serum, or HC serum supplemented with either SLE IgG or IFN- α , whereas the binding complex was reduced in SLE serum mixed with IFNAR-neutralizing antibodies or depleted of IgG (Extended Data Fig. 9b).

Finally, short interfering RNA (siRNA) knockdown of CREM α in neutrophil-like HL60 cells significantly abrogated GPX4 inhibition by SLE serum, autoantibodies or IFN- α ; in contrast, overexpression of CREM α decreased GPX4 expression (Extended Data Fig. 9c–e), supporting that CREM α is a key regulator upstream of GPX4 in neutrophils. As expected, HL60 cells stimulated with these factors displayed consistent changes in lipid-ROS (Extended Data Fig. 9f).

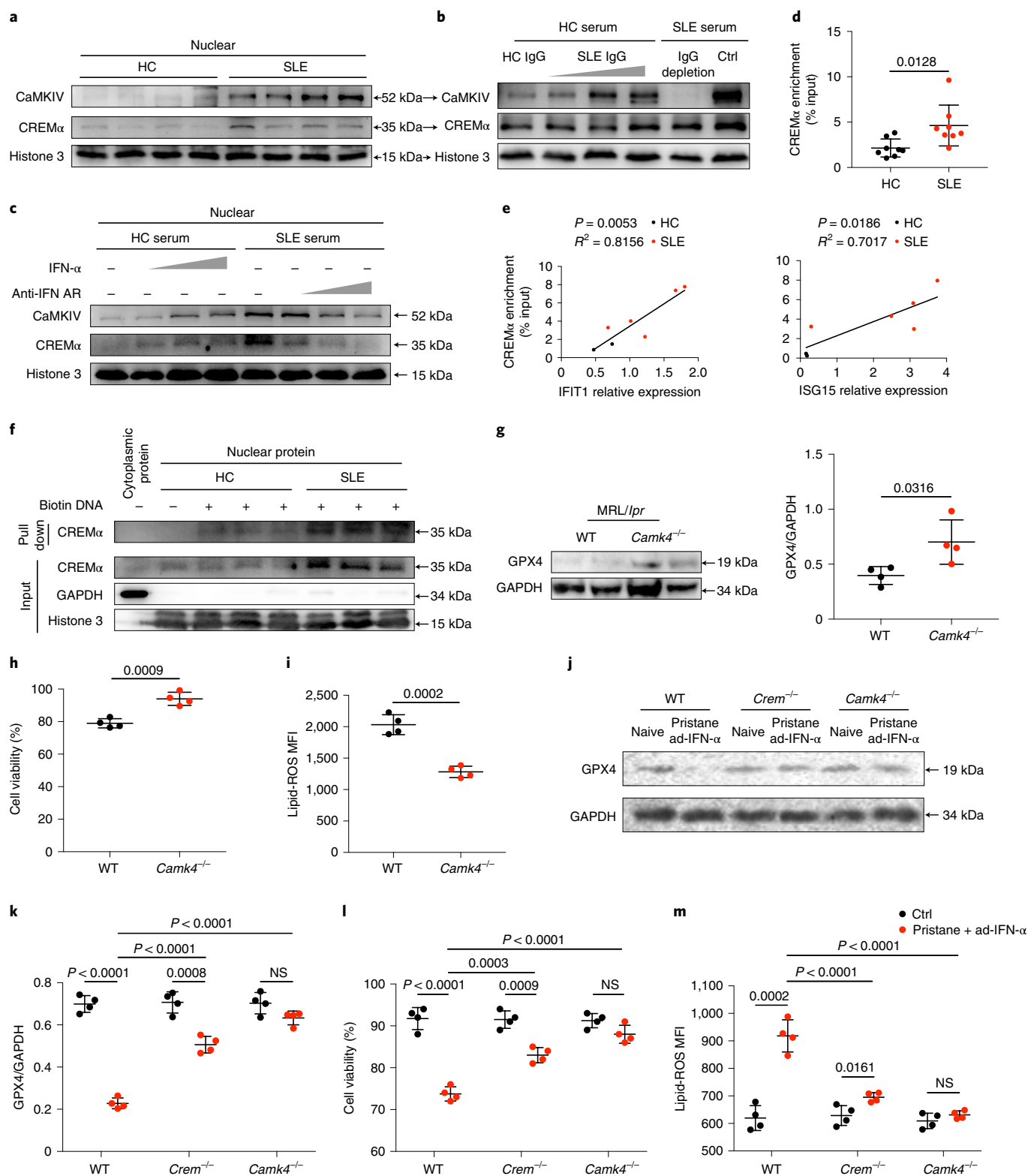
To validate the CREM α /CaMKIV axis in neutrophil ferroptosis in vivo, we examined neutrophils in *Camk4*^{-/-} MRL/*lpr* mice and observed higher levels of GPX4 and cell viability and lower lipid-ROS (Fig. 7g–i) compared with matched wild-type controls, confirming that CaMKIV deficiency promoted GPX4 expression and reduced neutrophil ferroptosis. Furthermore, we induced lupus-like disease in wild-type, CREM-deficient (*CreM*^{-/-}) and CaMKIV-deficient (*Camk4*^{-/-}) mice on the C57BL/6 background by administering pristane and adenovirus IFN- α (refs. 31,32).

Fig. 7 | IFN- α and SLE IgG suppress the transcription of GPX4 by promoting binding of CREM to the *Gpx4* promoter. **a**, Western blot analysis of nuclear accumulation of CREM α and CaMKIV in neutrophils isolated from HCs and patients with SLE. **b,c**, SLE IgG (1.2, 2.4, 3.6 g l⁻¹) (**b**) and IFN- α (10³, 10⁴, 10⁵ U ml⁻¹) (**c**) at different concentrations increased nuclear accumulation of CREM α and CaMKIV. **d**, SLE serum increased DNA binding of CREM α to *Gpx4* promoter area by ChIP analysis ($n=8$). **e**, Intracellular IFIT1 and ISG15 expression correlated positively with the enrichment of CREM α in the *Gpx4* promoter region. **f**, The interaction between the *Gpx4* promoter and CREM α by DNA pulldown assay. **g**, Western blot analysis of GPX4 in neutrophils isolated from WT and *Camk4*^{-/-} MRL/*lpr* mice at 18 weeks of age ($n=4$). **h**, Dot plots show flow cytometry quantification of neutrophil viability in WT and *Camk4*^{-/-} MRL/*lpr* mice at 18 weeks of age ($n=4$). **i**, Flow cytometry quantification of lipid-ROS in neutrophils from WT and *Camk4*^{-/-} MRL/*lpr* mice ($n=4$). **j–m**, WT, *CreM*^{-/-} and *Camk4*^{-/-} mice were first administered with pristane (intraperitoneally, 0.5 ml per mouse) for autoantibody induction and 2 months later intravenously with 2×10^9 p.f.u. adenovirus IFN- α (ad-IFN- α) to overexpress IFN- α in vivo. One more month after ad-IFN- α administration, mice were euthanized and GPX4 expression (**j**, western blot; **k**, quantification analysis), cell viability (**l**) and lipid-ROS (**m**) in circulating neutrophils isolated from indicated mice were analyzed ($n=4$). Data are shown as mean \pm s.d. NS, $P > 0.05$. Two-tailed unpaired Student's *t*-test was applied.

As expected, the combined effect of autoantibodies and IFN- α significantly decreased neutrophil GPX4 expression and viability and increased the production of lipid-ROS in wild-type but not *CreM α* ^{-/-} and *Camk4*^{-/-} mice (Fig. 7j–m). Together, our findings demonstrate that autoantibodies and IFN- α in SLE promote the nuclear translocation of CREM α and its binding to the *Gpx4* promoter in neutrophils, thus suppressing GPX4 expression and resulting in ferroptosis which contributes to disease development (Extended Data Fig. 10).

Discussion

Herein, we verified the key role of GPX4 in neutrophil ferroptosis and identified two pivotal factors, serum autoantibodies and IFN- α , which were responsible for neutropenia in SLE by inducing neutrophil ferroptosis through the activation of the CaMKIV/CREM α axis. The increased nuclear translocation of CaMKIV/CREM α led to the reduction of GPX4 accompanied by increased intracellular lipid-ROS, which finally resulted in neutrophil ferroptosis.



The pathogenic role of neutrophil ferroptosis in SLE was further documented in vivo by the findings that genetic haploinsufficiency of *Gpx4* in neutrophils led to the development of lupus-like disease in mice, whereas approaches to reduce neutrophil ferroptosis significantly mitigated disease development in lupus-prone mice.

The immune system is poised to recognize and respond to a plethora of dying cells, components of which are potentially immunostimulatory and capable of triggering autoimmunity³³. Short-lived neutrophils, the most abundant innate immune cells, represent one dominant source of dying cells in the daily burden³⁴. In SLE, neutrophils are prone to cell death and the absolute numbers decrease markedly³. Increased levels of neutrophil NETosis have been reported in patients with SLE³⁵. However, in our study, by carefully characterizing the pattern of neutrophil death in SLE, we demonstrated that ferroptosis is the major form of neutrophil death, although the contribution of NETosis cannot be excluded. Collectively, our data extend previous understanding of cell ferroptosis, which has been proposed to be associated with ischemic injury and degenerative and neoplastic diseases, and provide a missing link between neutropenia and inflammation in SLE^{9,10}.

Unlike the far better understood programmed cell death processes such as necroptosis and pyroptosis^{36,37}, ferroptosis and its exact role in inflammation and autoimmunity remain largely unknown. Two ways of quenching lipid peroxidation, that is, excessive oxidative modification of polyunsaturated fatty acids and the inhibition of GPX4, have been shown to induce cellular ferroptosis³⁸. Here, serum IgG and IFN- α have been documented to induce neutrophil ferroptosis in patients with SLE by inhibiting GPX4 expression. However, further efforts are needed to explore additional ferroptosis triggers in SLE, including iron and lipid metabolites and also other potential signaling molecules, such as VDAC2/3, nuclear factor E2-related factor 2 (NRF2), NADPH oxidase (NOX) and p53 (ref. ³⁸). Of note, vitamin E suppresses autoantibody production in lupus³⁹, which may be explained by its antioxidant effects to protect neutrophils away from ferroptosis. The immunogenicity of regulated cell death is critically dependent on the production of damage-associated molecular patterns (DAMPs)⁴⁰. Previous studies have indicated that ferroptosis results in the release of DAMPs, such as HMGB1 and LL-37 (ref. ⁴¹). By studying neutrophil death in SLE, we provide a model in which chronically elevated levels of autoantibodies and type I IFNs in patients with SLE provoke neutrophil ferroptosis, which through the release of autoantigens generates a positive feedback loop by providing stimuli to autoreactive B cells and pDCs to produce autoantibodies and type I IFNs. However, further studies are needed to delineate in detail mechanisms whereby neutrophil ferroptosis boosts inflammation in autoimmune diseases and especially in SLE. In addition, ferroptosis of other tissue-resident cells may contribute to the expression of autoimmune diseases. Previously, ferroptosis was demonstrated to account for neuronal cell death in patients with multiple sclerosis and mice immunized to develop encephalomyelitis⁴².

In summary, whereas most current theories concerning the induction of autoimmune diseases implicate the generation of autoreactive T and B lymphocytes, our findings propose a paradigm which places neutrophil ferroptosis at the center of the pathogenesis of SLE and highlights the importance of targeting GPX4 transcription and neutrophil ferroptosis in the treatment of lupus.

Online content

Any methods, additional references, Nature Research reporting summaries, source data, extended data, supplementary information, acknowledgements, peer review information; details of author contributions and competing interests; and statements of data and code availability are available at <https://doi.org/10.1038/s41590-021-00993-3>.

Received: 16 July 2020; Accepted: 7 July 2021;
Published online: 12 August 2021

References

1. Tsokos, G. C. Systemic lupus erythematosus. *N. Engl. J. Med.* **365**, 2110–2121 (2011).
2. Lisnevskaja, L., Murphy, G. & Isenberg, D. Systemic lupus erythematosus. *Lancet* **384**, 1878–1888 (2014).
3. Garcia-Romo, G. S. et al. Netting neutrophils are major inducers of type I IFN production in pediatric systemic lupus erythematosus. *Sci. Transl. Med.* **3**, 73ra20 (2011).
4. Bosch, X. Systemic lupus erythematosus and the neutrophil. *N. Engl. J. Med.* **365**, 758–760 (2011).
5. Dixon, S. J. et al. Ferroptosis: an iron-dependent form of nonapoptotic cell death. *Cell* **149**, 1060–1072 (2012).
6. Yang, W. S. et al. Regulation of ferroptotic cancer cell death by GPX4. *Cell* **156**, 317–331 (2014).
7. Alim, I. et al. Selenium drives a transcriptional adaptive program to block ferroptosis and treat stroke. *Cell* **177**, 1262–1279.e25 (2019).
8. Ingold, I. et al. Selenium utilization by GPX4 is required to prevent hydroperoxide-induced ferroptosis. *Cell* **172**, 409–422.e421 (2018).
9. Friedmann Angeli, J. P. et al. Inactivation of the ferroptosis regulator Gpx4 triggers acute renal failure in mice. *Nat. Cell Biol.* **16**, 1180–1191 (2014).
10. Do Van, B. et al. Ferroptosis, a newly characterized form of cell death in Parkinson's disease that is regulated by PKC. *Neurobiol. Dis.* **94**, 169–178 (2016).
11. Matsushita, M. et al. T cell lipid peroxidation induces ferroptosis and prevents immunity to infection. *J. Exp. Med.* **212**, 555–568 (2015).
12. van Vollenhoven, R. F. et al. Efficacy and safety of ustekinumab, an IL-12 and IL-23 inhibitor, in patients with active systemic lupus erythematosus: results of a multicentre, double-blind, phase 2, randomised, controlled study. *Lancet* **392**, 1330–1339 (2018).
13. ter Borg, E. J., Horst, G., Hummel, E. J., Limburg, P. C. & Kallenberg, C. G. Measurement of increases in anti-double-stranded DNA antibody levels as a predictor of disease exacerbation in systemic lupus erythematosus. A long-term, prospective study. *Arthritis Rheum.* **33**, 634–643 (1990).
14. Pisetsky, D. S. Anti-DNA antibodies—quintessential biomarkers of SLE. *Nat. Rev. Rheumatol.* **12**, 102–110 (2016).
15. Lood, C. et al. Neutrophil extracellular traps enriched in oxidized mitochondrial DNA are interferogenic and contribute to lupus-like disease. *Nat. Med.* **22**, 146–153 (2016).
16. Papayannopoulos, V., Metzler, K. D., Hakkim, A. & Zychlinsky, A. Neutrophil elastase and myeloperoxidase regulate the formation of neutrophil extracellular traps. *J. Cell Biol.* **191**, 677–691 (2010).
17. Stockwell, B. R. et al. Ferroptosis: a regulated cell death nexus linking metabolism, redox biology, and disease. *Cell* **171**, 273–285 (2017).
18. Friedmann Angeli, J. P. et al. Inactivation of the ferroptosis regulator Gpx4 triggers acute renal failure in mice. *Nat. Cell Biol.* **16**, 1180–1191 (2014).
19. Sun, Y., Zheng, Y., Wang, C. & Liu, Y. Glutathione depletion induces ferroptosis, autophagy, and premature cell senescence in retinal pigment epithelial cells. *Cell Death Dis.* **9**, 753 (2018).
20. Cohen, P. L. & Eisenberg, R. A. *Lpr* and *gld*: single gene models of systemic autoimmunity and lymphoproliferative disease. *Annu. Rev. Immunol.* **9**, 243–269 (1991).
21. Dubois, E. L., Horowitz, R. E., Demopoulos, H. B. & Teplitz, R. NZB/NZW mice as a model of systemic lupus erythematosus. *JAMA* **195**, 285–289 (1966).
22. Ginzler, E. M. et al. Mycophenolate mofetil or intravenous cyclophosphamide for lupus nephritis. *N. Engl. J. Med.* **353**, 2219–2228 (2005).
23. Alim, I. et al. Selenium drives a transcriptional adaptive program to block ferroptosis and treat stroke. *Cell* **177**, 1262–1279.e25 (2019).
24. Ingold, I. et al. Selenium utilization by GPX4 is required to prevent hydroperoxide-induced ferroptosis. *Cell* **172**, 409–422.e21 (2018).
25. Clark, S. R. et al. Platelet TLR4 activates neutrophil extracellular traps to ensnare bacteria in septic blood. *Nat. Med.* **13**, 463–469 (2007).
26. Speckmann, B. et al. Induction of glutathione peroxidase 4 expression during enterocytic cell differentiation. *J. Biol. Chem.* **286**, 10764–10772 (2011).
27. De Cesare, D., Fimia, G. M. & Sassone-Corsi, P. Signaling routes to CREM and CREB: plasticity in transcriptional activation. *Trends Biochem. Sci.* **24**, 281–285 (1999).
28. Hedrich, C. M. et al. cAMP response element modulator α controls IL2 and IL17A expression during CD4 lineage commitment and subset distribution in lupus. *Proc. Natl Acad. Sci. USA* **109**, 16606–16611 (2012).
29. Hedrich, C. M., Rauen, T., Kis-Toth, K., Kytтары, V. C. & Tsokos, G. C. cAMP-responsive element modulator α (CREM α) suppresses IL-17F protein expression in T lymphocytes from patients with systemic lupus erythematosus (SLE). *J. Biol. Chem.* **287**, 4715–4725 (2012).
30. Juang, Y. T. et al. Systemic lupus erythematosus serum IgG increases CREM binding to the IL-2 promoter and suppresses IL-2 production through CaMKIV. *J. Clin. Invest.* **115**, 996–1005 (2005).

31. Triantafyllopoulou, A. et al. Proliferative lesions and metalloproteinase activity in murine lupus nephritis mediated by type I interferons and macrophages. *Proc. Natl Acad. Sci. USA* **107**, 3012–3017 (2010).
32. Zhuang, H. et al. Toll-like receptor 7-stimulated tumor necrosis factor α causes bone marrow damage in systemic lupus erythematosus. *Arthritis Rheumatol.* **66**, 140–151 (2014).
33. Kolb, J. P., Oguin, T. H. 3rd, Oberst, A. & Martinez, J. Programmed cell death and inflammation: winter is coming. *Trends Immunol.* **38**, 705–718 (2017).
34. Tsokos, G. C., Lo, M. S., Costa Reis, P. & Sullivan, K. E. New insights into the immunopathogenesis of systemic lupus erythematosus. *Nat. Rev. Rheumatol.* **12**, 716–730 (2016).
35. Ren, Y. et al. Increased apoptotic neutrophils and macrophages and impaired macrophage phagocytic clearance of apoptotic neutrophils in systemic lupus erythematosus. *Arthritis Rheum.* **48**, 2888–2897 (2003).
36. Shi, J. et al. Cleavage of GSDMD by inflammatory caspases determines pyroptotic cell death. *Nature* **526**, 660–665 (2015).
37. Sun, L. et al. Mixed lineage kinase domain-like protein mediates necrosis signaling downstream of RIP3 kinase. *Cell* **148**, 213–227 (2012).
38. Stockwell, B. R. et al. Ferroptosis: a regulated cell death nexus linking metabolism, redox biology, and disease. *Cell* **171**, 273–285 (2017).
39. Maeshima, E., Liang, X. M., Goda, M., Otani, H. & Mune, M. The efficacy of vitamin E against oxidative damage and autoantibody production in systemic lupus erythematosus: a preliminary study. *Clin. Rheumatol.* **26**, 401–404 (2007).
40. Legrand, A. J., Konstantinou, M., Goode, E. F. & Meier, P. The diversification of cell death and immunity: *memento mori*. *Mol. Cell* **76**, 232–242 (2019).
41. Martin-Sanchez, D. et al. Ferroptosis, but not necroptosis, is important in nephrotoxic folic acid-induced AKI. *J. Am. Soc. Nephrol.* **28**, 218–229 (2017).
42. Hu, C. L. et al. Reduced expression of the ferroptosis inhibitor glutathione peroxidase-4 in multiple sclerosis and experimental autoimmune encephalomyelitis. *J. Neurochem.* **148**, 426–439 (2019).

Publisher's note Springer Nature remains neutral with regard to jurisdictional claims in published maps and institutional affiliations.

© The Author(s), under exclusive licence to Springer Nature America, Inc. 2021

Methods

Ethics statement. Informed consent was obtained from all human participants. Medical and economic support were provided for participants. All in vivo experiments were performed according to the guidance of the German Animal Welfare Law. Our study was approved by the Institutional Review Board and Animal Care and Use Committee of Peking Union Medical College Hospital (PUMCH) (JS-1196), Beth Israel Deaconess Medical Center's Institutional Review Board (2006P000298) and the Animal Care and Use Committee (088-2015).

Chemicals, cytokines and antibodies. Chemicals and cytokines used were as follows: recombinant human IFN α 2b (11100-1, PBL assay science), RSL-3 (S8155, Selleck), LPX-1 (S7699, Selleck), DFO (S5742, Selleck), Nec-1 (S8037, Selleck), NSA (S8251, Selleck), Z-VAD-FMK (S7023, Selleck), phorbol 12-myristate 13-acetate (PMA) (P8139, Sigma), GSK2795039 (HY-18950, MedChem Express), APX-115 (HY-120801, MedChem Express), Cl-amidine (506282, Merck), β -ME (M6250, Sigma), dimethylsulfoxide (D8371, Solarbio), CTX (S2057, Selleck), BODIPY 581/591 C11 (D3861, Invitrogen), penicillin (Gibco), streptomycin (Gibco), lysing buffer (555899, BD Pharmingen), DAPI (S2110, Solarbio), 7AAD (559925, BD Pharmingen), PI (P1304MP, Thermo Scientific), SYTOX Green (S7020, Invitrogen), Hoechst (62249, Thermo Scientific) and 16% formaldehyde (12606S, CST).

Antibodies used were as follows: anti-GPX4 (EPNCIR144, ab125066, Abcam; 1:1,000), anti-CaMKIV (ab3557, Abcam; 1:1,000), anti-histone 3 (ab1791, Abcam; 1:1,000), anti-C1q (4.8, ab182451, Abcam; 1:200), anti-neutrophil elastase (ab68672, Abcam; 1:200), anti-CREM (western blot: nbp2-16009, NOVUS; 1:1,000; chromatin immunoprecipitation (ChIP): A5624, Abclonal), anti-GAPDH (10494-1-AP, Proteintech; 1:1,000), anti- β -actin (BE0022, Easybio; 1:1,000), anti-SLC7A11 (26864-1-AP, Proteintech; 1:1,000), anti-histone H3 (citruilline R2) (EPR17703, ab176843, Abcam; 1:1,000), anti-Fc γ R3 β (MM0272-5L11, ab89207, Abcam; 1:1,000), anti-rabbit IgG-HRP (BE0101, Easybio; 1:5,000), anti-human IgG-HRP (BE0122, Easybio; 1:5,000), anti-mouse IgG-HRP (BE0102, Easybio; 1:5,000), PE conjugated anti-mouse Ly-6G (127607, Biolegend; 1:100), PE conjugated anti-human CD16 (561313, BD Pharmingen; 1:100), APC-conjugated anti-mouse/human CD11b (101212, Biolegend; 1:100), FITC-conjugated anti-mouse CD45 (103108, Biolegend; 1:100), FITC-conjugated anti-mouse Ly-6G&Ly-6C (553127, BD Pharmingen; 1:100), TruStain FcX anti-CD16/32 (422302, Biolegend; 1:100), goat pAb to mouse IgM Alexa Fluor 647 (ab150123, Abcam; 1:200), goat pAb to rabbit IgG Alexa Fluor 488 (ab150077, Abcam; 1:200), donkey pAb to rabbit IgG Alexa Fluor 647 (ab150075, Abcam; 1:100), goat anti-mouse IgG Alexa Fluor 594 (405326, Biolegend; 1:200), mouse monoclonal antibody against human interferon Alpha/Beta Receptor 1 (MMHAR-3, 21370-3, PBL Assay Science), anti-CXCL11 (ab9955, Abcam) and anti-human IL-12/23 (ustekinumab) (HY-P9909, Medchem Express).

Patients and HCs. Patients with SLE involved in this study were recruited from two cohorts, all fulfilling the diagnosis of SLE according to the criteria established by the American College of Rheumatology⁴⁵. Peripheral blood samples were obtained from new-onset untreated patients recruited from PUMCH. Patients with SLE were treated with standard-of-care medications including corticosteroid and immunosuppressants (such as mycophenolate mofetil or CTX) combined with hydroxychloroquine for at least 2 months, and post-treatment blood samples from these same patients with SLE were collected. WBC count, neutrophil count and anti-dsDNA were measured and analyzed on the day of blood collection. Disease activity was assessed by the modified SLEDAI-2000, calculated by omitting the immunologic variables including anti-dsDNA and serum complement concentrations from the SLEDAI-2000 (ref. 44).

Patients with SLE from another cohort (Caucasian $n=13$, African Americans $n=15$) were recruited from the Division of Rheumatology, Beth Israel Deaconess Medical Center.

Patients with RA, ankylosing spondylitis and Behcet's disease were recruited from PUMCH, and were all untreated and diagnosed according to the corresponding criteria⁴⁵⁻⁴⁷. Patients with infections or severe underlying disorders were also excluded. HCs were age- and sex-matched individuals without autoimmune, inflammatory or infectious diseases. Clinical characteristics and the treatment of patients with SLE included in the study are shown in Supplementary Tables 1-5 and 7.

Mice. Female MRL/Mpj and MRL.Mpj-Fas^{br} (MRL/lpr) mice were purchased from Shanghai Slack Laboratory, and maintained in the specific-pathogen-free conditions of PUMCH animal care facility.

NZB and NZW mice were purchased from the Jackson Laboratory and bred at Beijing Vital River Laboratory, and the first female generation (NZB/W F1) after crossbreeding was used for experiments.

The C57/B6-Gpx4^{fl/fl} (027964) and C57/B6-LysMcre (004781) mice were purchased from the Jackson Laboratory. The Gpx4^{fl/fl} allele has loxP sites flanking exons 2-4 of the Gpx4 gene. The LysMcre knock-in allele has a nuclear-localized Cre recombinase inserted into the first coding ATG of the lysozyme 2 gene (Ly2), both abolishing endogenous Ly2 gene function and placing NLS-Cre expression under the control of the endogenous Ly2 promoter/enhancer elements. The Gpx4^{fl/fl} mice were bred to the LysMcre mice to generate LysMcre⁺ Gpx4^{fl/wt} versions

of these strains. Gpx4^{fl/fl} and LysMcre⁺ Gpx4^{fl/wt} mice were used for experiments. All mice were bred and maintained in the animal facility of Beijing Vital River Laboratory under specific-pathogen-free conditions.

Female Camk4^{-/-} C57BL/6 mice were obtained from the Jackson Laboratory. Female Crem^{-/-} C57BL/6 and Camk4^{-/-} MRL/lpr mice were generated and maintained in the specific-pathogen-free animal facility at Beth Israel Deaconess Medical Center, Harvard Medical School. In all experiments, mice were carefully matched for age, sex, weight and genetic background.

In vivo experiments. In ferroptosis rescue experiments, LPX-1 (10 mg kg⁻¹), CTX (20 mg kg⁻¹) or 0.1 ml of dimethylsulfoxide (10%) was administered intraperitoneally to female MRL/Mpj and MRL/lpr mice every other day for 6 weeks beginning at 12 weeks of age. Urine was collected in the morning once a week. Mice were killed at 18 weeks of age, and spleen, kidneys, lymph nodes and peripheral blood were collected for analysis. For in vivo treatment, MRL/lpr mice were administered 0.1 ml of dimethylsulfoxide (10%), Cl-amidine (20 mg kg⁻¹), LPX-1 (10 mg kg⁻¹) or Cl-amidine (20 mg kg⁻¹) combined with LPX-1 (10 mg kg⁻¹) intraperitoneally every other day for 3 weeks starting at 12 weeks of age⁴⁸. Mice were euthanized at 15 weeks of age and spleen, lymph nodes, urine and peripheral blood were collected for analysis.

Peripheral blood and bone marrow were collected from 3- or 7-month-old NZB/W F1, Gpx4^{fl/fl} and Gpx4^{fl/wt} LysMcre⁺, MRL/Mpj and MRL/lpr mice. Neutrophils, lymphocytes and monocytes were isolated with Mouse Peripheral Blood Lymphocyte Separation Kit (P8620, Solarbio), Mouse Bone Marrow Neutrophil Isolation Kit (P8550, Solarbio), Mouse Peripheral Blood Neutrophil Separation Kit (P9201, Solarbio) and Mouse Peripheral Blood Monocyte Separation Kit (P5230, Solarbio).

Gpx4^{fl/fl} and Gpx4^{fl/wt} LysMcre⁺ mice were observed without interventions. Urine was collected in the morning once a month, and tail venous blood was collected for analysis. Absolute neutrophil counts were analyzed by flow cytometry. Neutrophils were isolated and cultured in complete medium supplemented with LPX-1 (1 μ M) for 16 h and assessed for cell viability and lipid-ROS.

Pristane-induced murine lupus: 2-month-old female wild-type, Crem^{-/-} and Camk4^{-/-} C57BL/6 mice were intraperitoneally administered with Pristane (0.5 ml per mouse, P2870, Sigma). After 2 months, 2 \times 10⁸ plaque-forming units (p.f.u.) of adenovirus IFN- α per mouse were intravenously administered and mice were euthanized 1 month later.

Cell isolation and in vitro culture. To isolate neutrophils and peripheral blood mononuclear cells, blood was layered on Ficoll-Hypaque density gradients and centrifuged, following the manufacturer's instructions. Erythrocytes were lysed with Lysing Buffer. Monocytes, B cells and pDCs were purified with CD14 microbeads (130050201, Miltenyi), CD19 microbeads (130050301, Miltenyi) and Plasmacytoid Dendritic Cells Isolation Kit II Human (130097415, Miltenyi), respectively. The preparation contained greater than 98% neutrophils as confirmed by flow cytometry using anti-CD16 and anti-CD11b. Cells were cultured in complete RPMI 1640 basic medium (Gibco) with 100 U ml⁻¹ penicillin, 100 μ g ml⁻¹ streptomycin and 20% serum from ten randomly selected patients with SLE or age- and sex-matched HCs, and incubated at 37 °C in a humidified atmosphere of 20% O₂ and 5% CO₂. IFN- α 2b (10³-10⁵ U ml⁻¹), anti-IFNAR1 (0.1-10 μ g ml⁻¹), anti-CXCL11 (0.1-10 μ g ml⁻¹), ustekinumab (0.1-10 μ g ml⁻¹), RSL-3 (10 μ M), LPX-1 (0.01-1 μ M), DFO (1-100 μ M), Nec-1 (0.01-1 μ M), NSA (0.01-1 μ M), Z-VAD (0.01-1 μ M), β -ME (10 or 50 μ M), PMA (50 nM), Cl-amidine (100 μ M), GSK2795039 (10 μ M) or APX-115 (5 μ M) was added in corresponding experiments. Neutrophils were cultured for 4-30 h for further analysis. Cultural supernatant of pDC and B cells was collected at 24 h and 72 h, respectively.

In relevant experiments, purified SLE IgG (1.2-3.6 g l⁻¹) was added to complete medium.

Quantification of NET formation by fluorescence microscopy. HC neutrophils were cultured in complete RPMI medium supplemented with 20% HC or SLE serum in the presence or absence of LPX-1 (1 μ M), Cl-amidine (100 μ M), IFN- α 2b (10³ U ml⁻¹) and SLE IgG (3.6 g l⁻¹) for 4 or 16 h at a density of 1 \times 10⁵ cells per well in 96-well plates. The release of NET DNA was measured with DAPI and PI or SYTOX Green and Hoechst using a fluorescence microscope (ZEISS). Neutrophils whose DNA area exceeded 400 μ m² were considered undergoing NETosis as previously described⁴⁹.

Cell viability quantification. The viability of freshly isolated or cultured neutrophils, monocytes and lymphocytes was determined by the Annexin V/7-AAD assay with the PE Annexin V Apoptosis Detection Kit I (559763, BD Pharmingen). Annexin V (-) and 7AAD (-) cells were considered living cells. Lactate dehydrogenase release was measured with the Cytotoxicity Detection Kit according to manufacturer's instructions (11644793001, Merck). The viability quantification by fluorescence microscopy was similar to NET quantification, measured with SYTOX Green and Hoechst.

IgG purification. SLE or HC IgG was purified using the ProteoExtract Albumin/IgG Removal Kit (122643, Merck) or Protein A/G (BE6868, Easybio) according

to the manufacturers' protocols. For kit-isolated IgG, 0.75 M NaHCO₃ was used to neutralize the pH of the eluent. IgG was enriched by centrifugal filters (UFC905096, Merck) and resuspended in PBS.

Transmission electron microscopy. Neutrophils freshly isolated or cultured with vehicle (dimethylsulfoxide) or RSL-3 (10 μM) for 4 h were fixed with 2.5% glutaraldehyde in 0.1 M Sorenson's buffer for 3 h, and then treated with 1% OsO₄ in 0.1 M Sorenson's buffer for 2 h. Enblock staining used 1% tannic acid. After dehydration through an ethanol series, neutrophils were embedded in LX-112 (Ladd Research Industries) and Embed-812 (EMS). The thinly cut sections were stained with 1% uranyl acetate and 0.4% lead citrate and examined under the TEM-1400 Plus electron microscope. Electron micrographs were taken at 5,000–50,000-fold magnification. Eight patients with SLE and six HCs were evaluated for mitochondrial vacuolization by electron microscopy. We randomly collected ten neutrophils per sample under a ×50,000 lens and counted the number of mitochondria with vacuoles for quantitative analysis. Images were optimized using Photoshop CC 2017 and Illustrator CC 2017 (Adobe).

Flow cytometry. For neutrophil percentage measurements, whole-blood cells of mice were stained with combinations of antibodies including anti-Ly-6G, anti-CD11b and anti-CD45 for 30 min on ice in staining buffer. For detection of intracellular GPX4 expression, cells were stained with anti-Ly-6G&Ly-6C and anti-GPX4 after fixation and permeabilization with Cytotfix/Cytoperm solution (554714, BD Pharmingen). After incubation for 2 h, cells were washed before being stained with anti-rabbit IgG Alexa Fluor 647. For the lipid-ROS detection, neutrophils were washed twice and incubated for 15 min with 2 μM C11-BODIPY (581/591). Afterward, neutrophils were washed twice and resuspended in PBS. Lipid-ROS was assessed by measuring the fluorescence change of C11-BODIPY at 488 nm using a BD FACS Aria II (BD Biosciences). Data were analyzed using FlowJo (v.10.4, Tree Star).

Multiplex cytokine detection. Cytokines and immunoglobulin in human and mouse plasma were measured with the LEGENDplex™ Mouse Th Cytokine Panel (740005, Biolegend), Mouse Immunoglobulin Isotyping Panel (740493, Biolegend), Human Cytokine Panel 2 (740102, Biolegend), Human Th Cytokine Panel (740721, Biolegend) and Human Proinflammatory Chemokine Panel (740003, Biolegend), following the manufacturers' instructions. Data analysis was carried out using LEGENDplex Data Analysis Software (v.8.0). Heatmaps were constructed using GraphPad Prism 7, and Venn diagrams completed on <http://bioinformatics.psb.ugent.be/>.

ELISA. Mouse serum was diluted 1:100 with assay buffer for anti-dsDNA detection and 1:25,000 for complement 3 detections. Assays were carried out with Mouse Anti-dsDNA IgG ELISA Kit (5120, Alpha Diagnostic Intl.) and Complement 3 ELISA Kit (6270, Alpha Diagnostic Intl.), following the manufacturer's protocols. Urine protein concentrations were detected using BCA Protein Assay Kit (23225, Thermo Scientific). IgG of B cell cultural supernatant was measured by the Human IgG ELISA Kit (E88-104, Bethyl).

Western blot and nuclear separation. Cells were lysed on ice using RIPA buffer (Huaxingbio) supplemented with a protease inhibitor and phosphatase inhibitor cocktail (78446, Thermo Scientific). Protein concentration of lysates was determined using the BCA Protein Assay Kit according to the manufacturers' instructions. Cell lysates were boiled for 10 min at 95 °C with SDS, and subjected to 12% SDS-PAGE, and then transferred to PVDF membranes (1620177, Bio-Rad). The membranes were blocked and then incubated with anti-GPX4, anti-CREM, anti-CaMKIV, anti-SLC7A11, anti-FcγR3β, anti-Histone 3, anti-GAPDH or anti-β-actin overnight at 4 °C. The membranes were washed and incubated with anti-rabbit or -mouse IgG-HRP for 1 h. Protein bands were visualized with the western blotting detection system Tanon-5200 (Bio-Tanon, China). Gray value analysis was done by ImageJ (v.1.50g, NIH) software. The nuclear content of cells was isolated and determined by Cytoplasmic & Nuclear Extraction Kits (SC-003, Invent) according to the manufacturer's instructions.

Immunofluorescence. For NET staining, freshly isolated neutrophils (10⁵ cells) from HCs and patients with SLE were transferred into a 24-well plate with BioCoat poly-L-lysine slides (Corning), and cultured in complete RPMI 1640 basic medium with 20% HC or SLE serum in the presence or absence of LPX-1 (1 μM) and PMA (50 nM). After incubation at 37 °C for 4 h, cells were fixed with 4% paraformaldehyde. NETs were stained using anti-neutrophil elastase for 2 h, and then anti-rabbit IgG Alexa Fluor 488. Slides were mounted with anti-quenching agent containing DAPI.

Kidneys were taken from mice, fixed in 4% paraformaldehyde, embedded in paraffin and stained with periodic acid-Schiff. The second kidney from each mouse was frozen in O.C.T. compound (Tissue-Tek) at –80 °C, and used for assessment of immune complex deposition. The 6-μm sections of snap-frozen kidney tissue were treated with blocking buffer (100 mM Tris-HCl, pH 8.0, 0.3% Triton X-100, 2% BSA and 50 μg ml⁻¹ goat nonspecific IgG) for 1 h. Afterward, the tissue was stained with anti-mouse IgG Alexa Fluor 594, anti-mouse IgM

Alexa Fluor 647 or anti-C1q plus anti-rabbit IgG Alexa Fluor 488. Coverslips were mounted in anti-quenching agent with DAPI. All slides were examined with the A1 HD25/A1R HD25 Nikon confocal laser microscope (Nikon, Japan). Images were optimized using Photoshop CC 2017 and Illustrator CC 2017 (Adobe).

RNA isolation and quantitative PCR. Total RNA was extracted with TRIzol (10296010, Invitrogen), and converted to complementary DNA using PrimeScript RT Master Mix (RR036A, Takara Bio). Quantitative PCR (qPCR) was carried out with the Applied Biosystems 7500 using SYBR Premix Ex Taq™ II (RR820A, Takara Bio). The relative RNA expression level was normalized to GAPDH messenger RNA according to the $\Delta\Delta C_t$ calculation method³⁰.

The primers used were as follows:

GAPDH

Forward: 5'-TCAACGACCACTTTGTCAAGCTCA-3'

Reverse: 5'-GCTGGTGGTCCAGGGGTCTTACT-3'

GPX4

Forward: 5'-GAGGCAAGACCGAAGTAACTAC-3'

Reverse: 5'-CCGAAGTGGTTACACGGGAA-3'

CREM

Forward: 5'-CGTCGACATCTTTGGCAGC-3'

Reverse: 5'-ATGACCATTGAAACAGTTGAATCCCA-3'

ISG15

Forward: 5'-TGGACAAATGCGACGAACCTC-3'

Reverse: 5'-TCAGCCGTACTCTGATAGGTG-3'

IFIT1

Forward: 5'-GCGCTGGGTATGCGATCTC-3'

Reverse: 5'-CAGCCTGCCTTAGGGGAAG-3'

RNA-seq analysis. Total RNA of freshly isolated HC or SLE neutrophils was extracted with TRIzol, and subjected to RNA-seq analysis. RNA-seq was performed by the Novogene Experimental Department using the Illumina HiSeq 4000 platform. Raw reads of fastq format were firstly processed through in-house perl scripts and all the downstream analyses were based on the clean data with high quality. An index of the reference genome was built using bowtie2 v.2.2.8 and paired-end clean reads were aligned to the reference genome using HISAT2 v.2.0.4. The mapped reads of each sample were assembled by StringTie (v.1.3.1). Cuffdiff (v.2.1.1) was used to calculate fragments per kilobase million (FPKM) of coding genes in each sample and provided statistical routines for determining differential expression using a model based on the negative binomial distribution. Transcripts with a *P*-adjust < 0.05 were assigned as differentially expressed.

DNA pulldown. Nuclear lysates were obtained from HC or SLE neutrophils as described above. Biotin-labeled *Gpx4* promoter DNA was synthesized by Guangzhou RiboBio (forward: 5'-ATTGGCTGACGTCG-3'; reverse: 5'-CGACGTCAGCCCAAT-3'). The biotinylated promoter DNA oligos were annealed and incubated with nuclear lysates at room temperature for 1 h in binding buffer (10 mM Tris, 1 mM KCl, 1% NP-40, 1 mM EDTA, 5% glycerol). Afterward, M-280 streptavidin Dynabeads (10004D, Invitrogen) were added and incubated for 2 h at 4 °C with rotation. After three washes with binding buffer, the GPX4-promotor-binding proteins were eluted by boiling and analyzed by western blot.

ChIP analysis. ChIP analysis was conducted on neutrophils with anti-CREM (Abclonal) and the assay was performed according to the manufacturer's instructions (9003, CST). Each sample (4 × 10⁶ cells) was crosslinked with 1% formaldehyde and then subjected to nuclear extraction and chromatin digestion with micrococcal nuclease. Sonication was used for complete lysis of nuclei (10-s pulse and 30-s pause; five cycles). The efficiency of chromatin digestion was determined by nucleic acid electrophoresis. For immunoprecipitation, digested chromatin was incubated with 10 μg of antibodies for 6 h at 4 °C with rotation. Afterward, magnetic beads were added to the immunoprecipitation reaction for 2 h at 4 °C with rotation. After washing four times, immunoprecipitated chromatin DNA was eluted. Fold enrichment was quantified using qPCR with SYBR Green Realtime PCR Master Mix (QPK-201, TOYOBO) and calculated as a percentage of input chromatin (% input). The primer sequences of *Gpx4* promoter were 5'-ACAAGTCCGACGTCGGT-3' (forward) and 5'-ATTGGTCAGACGCTCGGTGT-3' (reverse).

RNA interference and plasmids. HL60 cells (KG141, Keygen) were transfected with siRNA (20 nmol ml⁻¹) or plasmids (1 μg ml⁻¹) of *Crem* (NCBI Gene ID: 1390) and *Fcγr3b* (NCBI Gene ID: 2215). 293T cells (CL-0005, Procell) were transfected with plasmids (1 μg ml⁻¹) of *Slc7a11* (NCBI Gene ID: 23657). Full-length sequences were obtained from Sangon Biotech and then cloned into pcDNA3.1 vector. For transfection, cells were treated with the Gene Pulser II electroporation system (Bio-Rad), the 4D-Nucleofector X Kit L (V4XP-3024, LONZA,) or lipo-2000 (11668-027, Invitrogen) according to the manufacturer's instructions. The efficiency of interference or overexpression was determined by qPCR or western blot. The corresponding siRNAs used were as follows:

CREM:

siRNA-1

Forward: 5'-GCAGAAUCAGAAGGUGUAATT-3'

Reverse: 5'-UUACACCUUCUGAUUCUGCTT-3'
siRNA-2
Forward: 5'-GGUGGAACAAUCCAGAUUUTT-3'
Reverse: 5'-AAAUCUGGAUUGUCCACCTT-3'
siRNA-3
Forward: 5'-CCCAGGAUCUGAUGGUGUUTT-3'
Reverse: 5'-AACACCAUCAGAUCUGGGTT-3'

Statistics and reproducibility. Each experiment was repeated independently more than three times, and similar results were obtained. All data were analyzed using GraphPad Prism 7 software. Shapiro–Wilk test was used for normal distribution verification. For data with a normal distribution and homogeneity of variance, the independent sample *t*-test was used to compare differences between two groups. In some experiments, a paired Student's *t*-test was applied as indicated. For data with non-normal distribution, Mann–Whitney tests were applied. Correlations were calculated using Pearson rank correlation analysis. Sample sizes were determined on the basis of previous experiments using similar methodologies and are detailed in each figure legend. For *in vivo* studies, mice were randomly assigned to treatment groups. Data in figure legends are presented as mean \pm s.d. values or median with interquartile range. $P < 0.05$ was considered significant.

Reporting Summary. Further information on research design is available in the Nature Research Reporting Summary linked to this article.

Data availability

All raw source data for all experiments included in this study are provided. RNA sequencing data that support the findings of this study have been deposited with the Gene Expression Omnibus (GEO) repository under accession number [GSE153781](https://www.ncbi.nlm.nih.gov/geo/query/acc.cgi?acc=GSE153781). Correspondence and requests for materials should be addressed to zxpumch2003@sina.com. Source data are provided with this paper.

References

43. Hochberg, M. C. Updating the American College of Rheumatology revised criteria for the classification of systemic lupus erythematosus. *Arthritis Rheum.* **40**, 1725 (1997).
44. Uribe, A. G. et al. The Systemic Lupus Activity Measure-Revised, the Mexican Systemic Lupus Erythematosus Disease Activity Index (SLEDAI), and a modified SLEDAI-2K are adequate instruments to measure disease activity in systemic lupus erythematosus. *J. Rheumatol.* **31**, 1934–1940 (2004).
45. Kay, J. & Upchurch, K. S. ACR/EULAR 2010 rheumatoid arthritis classification criteria. *Rheumatology (Oxford)* **51**, vi5–vi9 (2012).
46. van der Linden, S., Valkenburg, H. A. & Cats, A. Evaluation of diagnostic criteria for ankylosing spondylitis. A proposal for modification of the New York criteria. *Arthritis Rheum.* **27**, 361–368 (1984).
47. International Team for the Revision of the International Criteria for Behçet's Disease (ITR-ICBD). The International Criteria for Behçet's Disease (ICBD): a collaborative study of 27 countries on the sensitivity and specificity of the new criteria. *J. Eur. Acad. Dermatol. Venereol.* **28**, 338–347 (2014).
48. Knight, J. S. et al. Peptidylarginine deiminase inhibition disrupts NET formation and protects against kidney, skin and vascular disease in lupus-prone MRL/*lpr* mice. *Ann. Rheum. Dis.* **74**, 2199–2206 (2015).
49. Papayannopoulos, V., Metzler, K. D., Hakkim, A. & Zychlinsky, A. Neutrophil elastase and myeloperoxidase regulate the formation of neutrophil extracellular traps. *J. Cell Biol.* **191**, 677–691 (2010).
50. Livak, K. J. & Schmittgen, T. D. Analysis of relative gene expression data using real-time quantitative PCR and the $2^{-\Delta\Delta C_t}$ method. *Methods* **25**, 402–408 (2001).

Acknowledgements

This study was supported by National Natural Science Foundation of China grants no. 81788101 (to X.Z.) and no. 81630044 (to X.Z.); Chinese Academy of Medical Science Innovation Fund for Medical Sciences grants no. CIFMS2016-12M-1-003 (to X.Z.), no. 2017-12M-1-008 (to X.Z.), no. 2017-12M-3-011 (to X.Z.) and no. 2016-12M-1-008 (to X.Z.); Capital's Funds for Health Improvement and Research (grant no. 2020-2-4019) (to X.Z.); and NIH grants no. R01AR064350 (to G.C.T.) and no. R37AI049954 (to G.C.T.). We thank A. Davidson at Feinstein Institutes for Medical Research for providing the adenovirus IFN- α . We thank the staff of the Rheumatology and Immunology Laboratory and Medical Scientific Research Center in Peking Union Medical College Hospital (PUMCH) for providing experimental equipment. We thank the doctors at PUMCH, Anyang District Hospital of Henan Province, Xiangya Hospital, Huaian No.1 People's Hospital and People's Hospital of Xinjiang Uygur Autonomous Region for patient recruitment.

Author contributions

X.Z. and P.L. conceived the project and designed the experiments. P.L., M.J., K.L. and H.L. performed most of the experiments with help from X.X., Y.X. and S.K. Y.Z. and H.L. contributed to discussions. P.L., H.L. and P.E.L. wrote the manuscript. G.C.T. and X.Z. supervised work and acquired funding.

Competing interests

P.E.L. is an employee of AMPEL but has no competing interests with the content of this manuscript. All the authors declare no competing interests.

Additional information

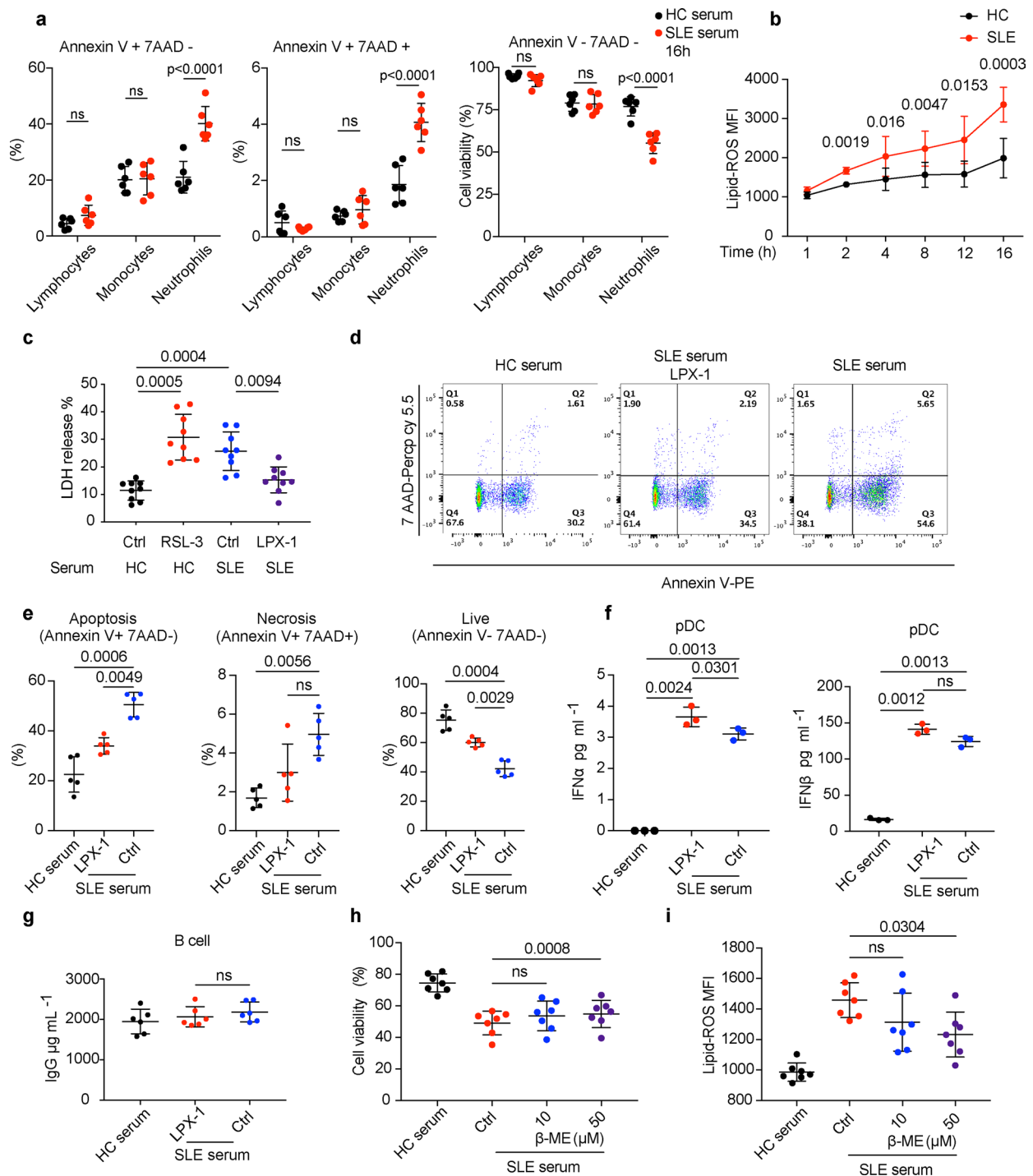
Extended data is available for this paper at <https://doi.org/10.1038/s41590-021-00993-3>.

Supplementary information The online version contains supplementary material available at <https://doi.org/10.1038/s41590-021-00993-3>.

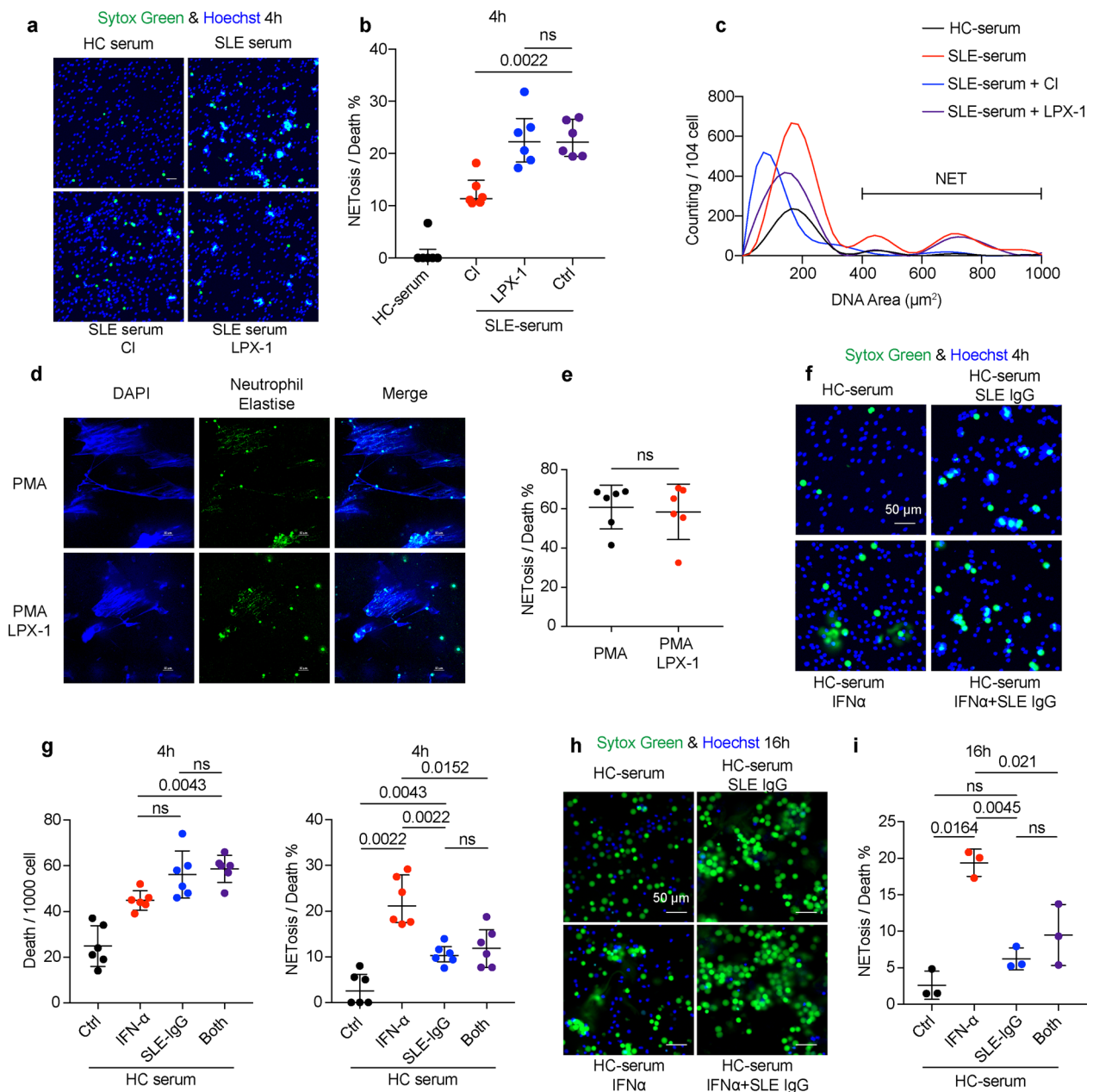
Correspondence and requests for materials should be addressed to P.E.L., G.C.T. or X.Z.

Peer review information *Nature Immunology* thanks Marcus Conrad, Christian Lood and Chandra Mohan for their contribution to the peer review of this work. Peer reviewer reports are available. L. A. Dempsey was the primary editor on this article and managed its editorial process and peer review in collaboration with the rest of the editorial team.

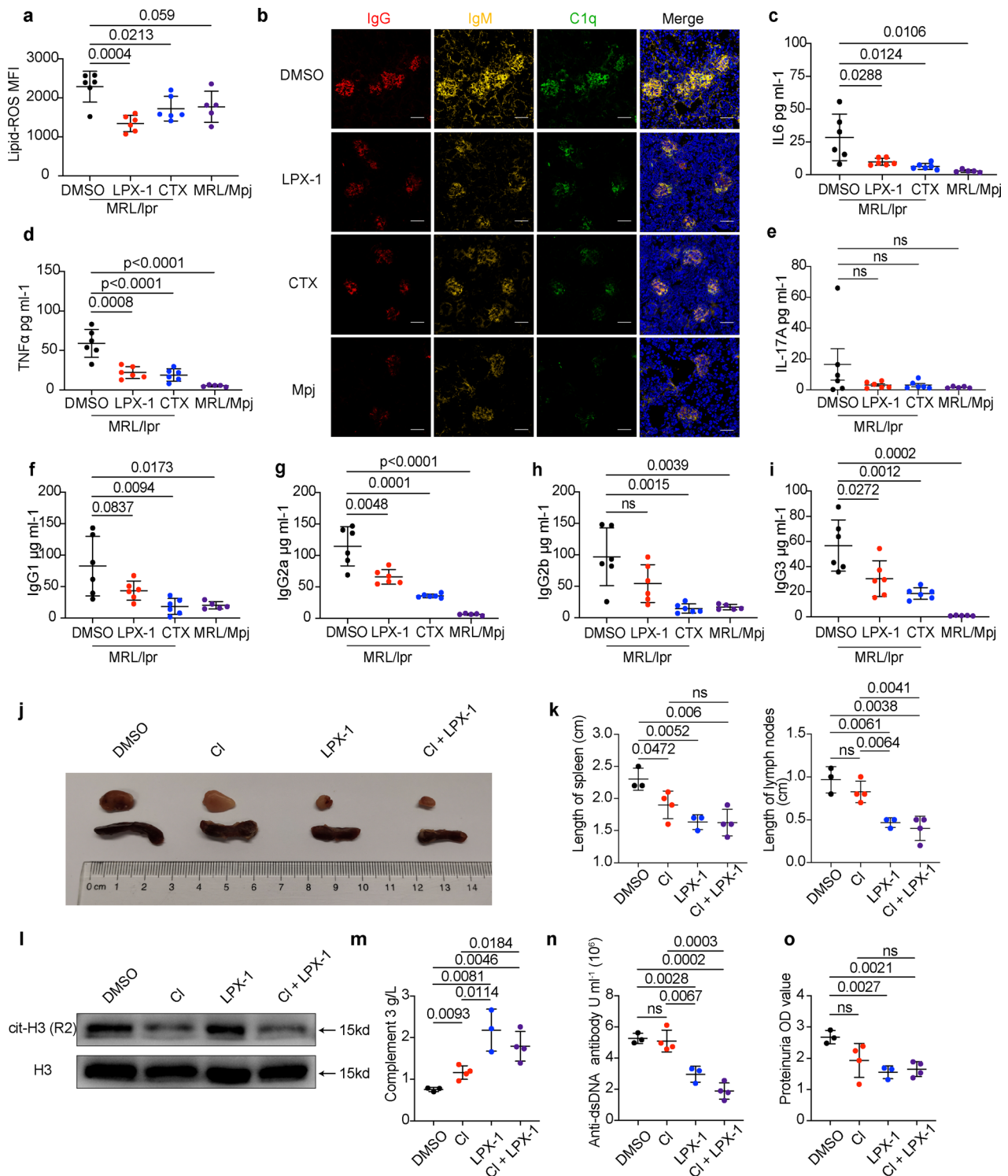
Reprints and permissions information is available at www.nature.com/reprints.



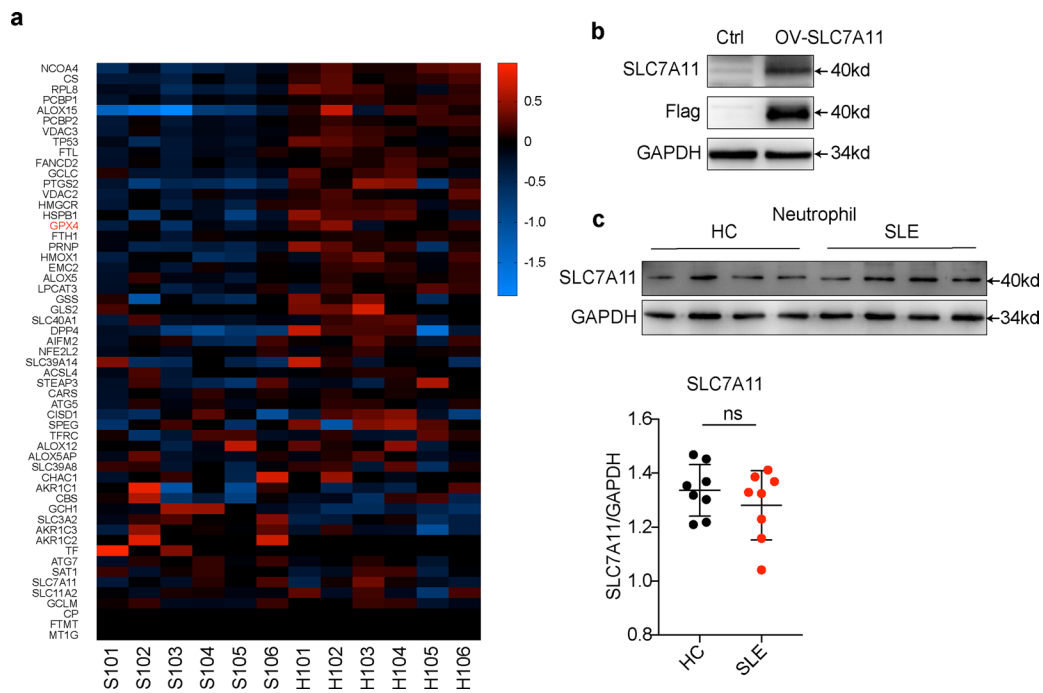
Extended Data Fig. 2 | Ferroptosis is restricted in neutrophils but not other cells in SLE and this could be reverted by addition of Ferroptosis specific inhibitors. **a**. Flow cytometry quantification of cell viability of HC lymphocytes, monocytes, and neutrophils cultured with 20% HC or SLE serum for 16 hours and the proportion of apoptotic (Annexin V + 7AAD⁻), necrotic (Annexin V + 7AAD⁺) and live (Annexin V - 7AAD⁻) cells in each subset was analyzed (n = 6). **b**. HC neutrophils were cultured with 20% HC or SLE serum, and lipid-ROS productions at different time points were detected (n = 3). **c**. Dot plots show cell viability analyzed by lactate dehydrogenase (LDH) release. HC neutrophils (n = 9) were cultured with 20% HC serum supplemented with RSL-3 (10 μ M) or SLE serum supplemented with LPX-1 (1 μ M) for 16 hours before analysis. **d-e**. Dot plots show flow cytometry quantification of the percentage of apoptotic, necrotic, and live cells. HC neutrophils (n = 5) were cultured with 20% HC or SLE serum in the presence or absence of LPX-1 (1 μ M) for 16 hours before analysis. **f-g**. HC B cells (n = 6) were cultured in 20% HC or SLE serum supplemented with LPX-1 for 72 hours, and plasmacytoid dendritic cells (pDC) (n = 3) were cultured for 24 hours, the level of IgG was assessed by ELISA and type I IFNs by flow cytometry individually. **h-i**. Dot plots show cell viability and lipid-ROS in HC neutrophils (n = 7) cultured with 20% HC or SLE serum supplemented with β -ME (10/50 μ M) for 16 hours. Data are shown as mean \pm SD. ns $p > 0.05$. Two-tailed paired Student's t-test was applied.



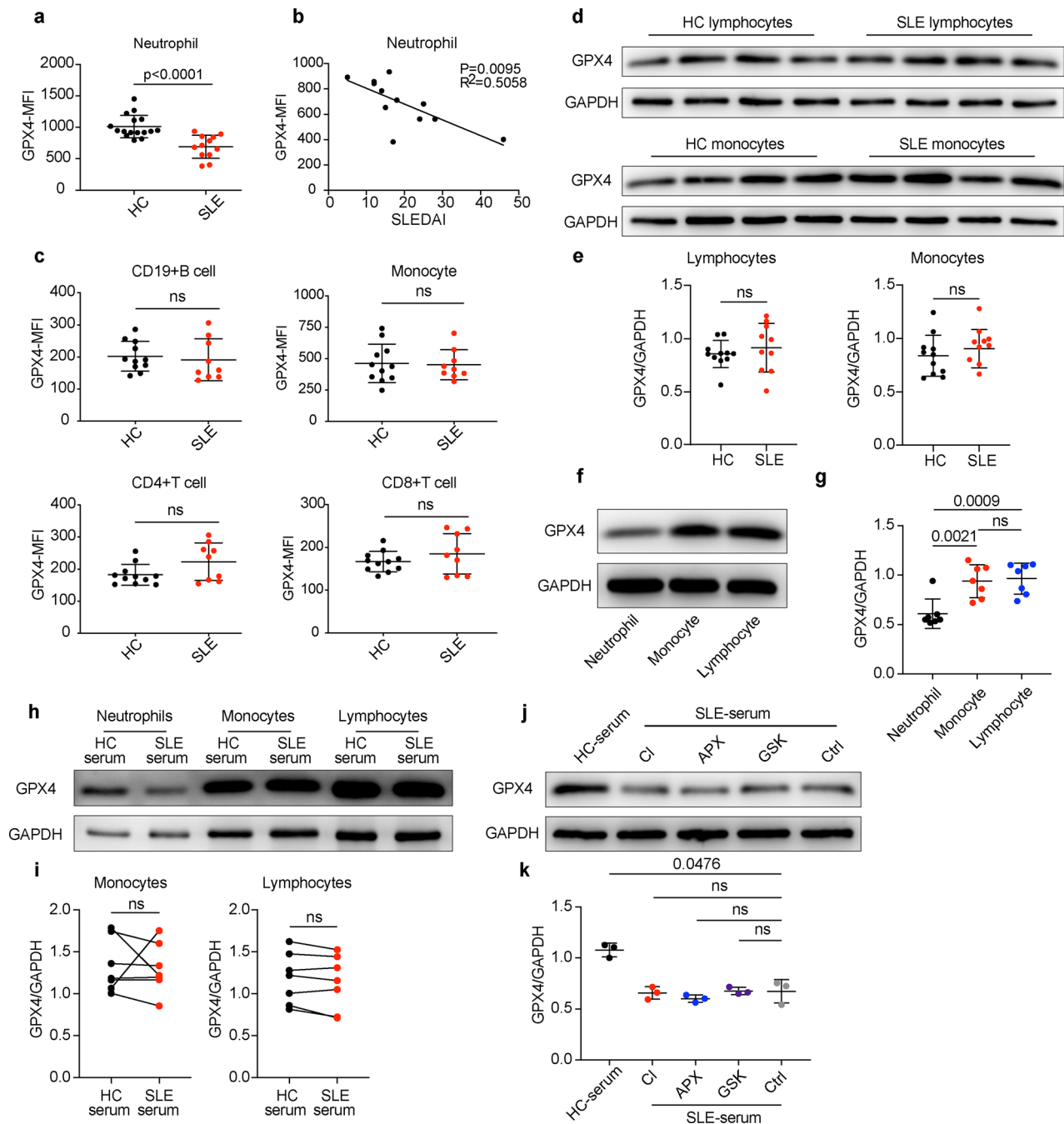
Extended Data Fig. 3 | The cooperative effects between IFN α and SLE IgG on cell death. **a-c.** HC neutrophils were cultured in the presence of HC or SLE serum with or without the addition of CI-amidine (CI) (peptidyl arginine deiminase 4 (PAD4) inhibitor, 100 μM), or LPX-1 (1 μM) for 4 or 16 hours and NETs were assessed in SYTOX Green+ cells based on morphology ($n=6$). Neutrophils with DNA area greater than 400 μm^2 were considered as NETs. Dot plots show the percentage of cells forming NETs in all dead neutrophils from the indicated group. **d-e.** Representative fluorescent images and related quantification of NETosis. HC neutrophils ($n=6$) were stimulated by PMA (50 nM) with or without LPX-1 (1 μM) for 4 hours. **f-i.** HC neutrophils were cultured with SLE IgG (3.6 g L^{-1}) and/or IFN- α (10^5 U ml^{-1}) for 4 or 16 hours and cells were stained with SYTOX Green for the detection of NETs. Dot plots show the immunofluorescence microscope quantification of NETosis in total dead neutrophils from the indicated group (4 h: $n=6$; 16 h: $n=3$). The scale bar represents 50 μm . Data are shown as mean \pm SD. ns $p > 0.05$. Two-tailed paired Student's t-test was applied.



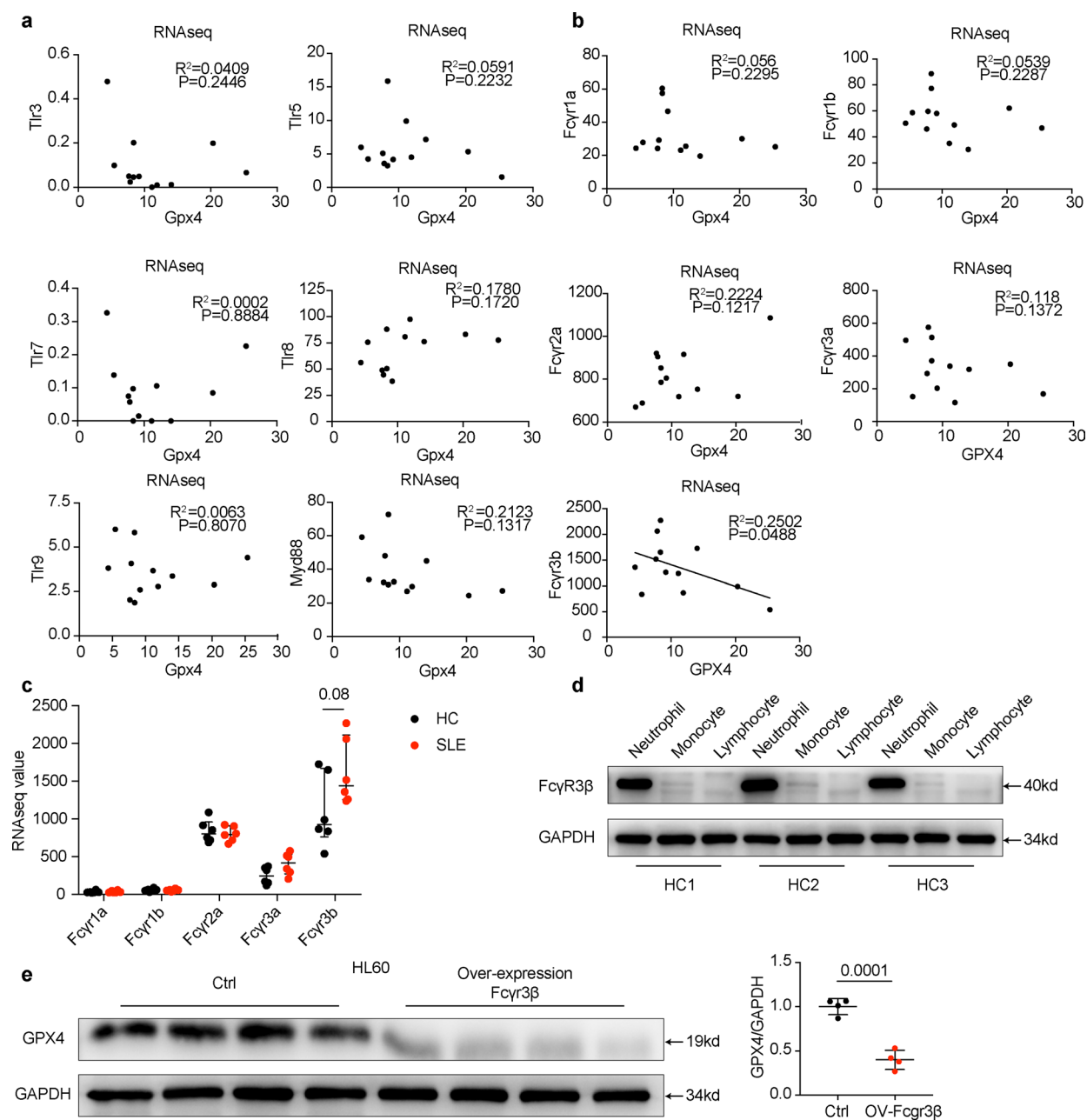
Extended Data Fig. 4 | The ferroptosis inhibitor ameliorates lupus progression with much better therapeutic effect compared to the NETosis inhibitor. **a-i.** MRL/lpr mice ($n=6$) were treated with DMSO (0.1 ml 10%), LPX-1 (10 mg/kg) or CTX (20 mg/kg) every other day at week 12 for 6 weeks, DMSO (0.1 ml 10%) was applied to sex-matched MRL/Mpj mice ($n=5$) as control. Mice were euthanized at 18 weeks of age for analysis. **(a)** Flow cytometry quantification of lipid ROS. **(b)** Representative immunofluorescent images of glomeruli stained with IgG (red), IgM (yellow), C1q (green), and DAPI (blue). **(c-e)** Flow cytometry quantification of plasma inflammatory factors and **(f-i)** plasma IgG. **j-o.** MRL/lpr mice (DMSO, LPX-1: $n=3$; CI, CI+LPX-1: $n=4$) were treated with DMSO, CI, LPX-1, or CI combined with LPX-1 every other day for 3 weeks starting at the age of week 12. Mice were euthanized at 15 weeks of age for analysis. **(j-k)** Representative images and related quantification of axillary spleens and lymph nodes. **(l)** Western blot analysis of cit-H3 in circulating neutrophils from mice subjected to the indicated treatment. **(m)** Dot plots show the ELISA assessment of serum complement 3. **(n)** Dot plots show the ELISA assessment of serum anti-dsDNA antibodies titers. **(o)** Dot plots shows the Bicinchoninic acid (BCA) assay of urine proteins. The scale bar represents 50 μ m. Data are shown as mean \pm SD. ns $p > 0.05$. Two-tailed unpaired Student's t -test was applied.



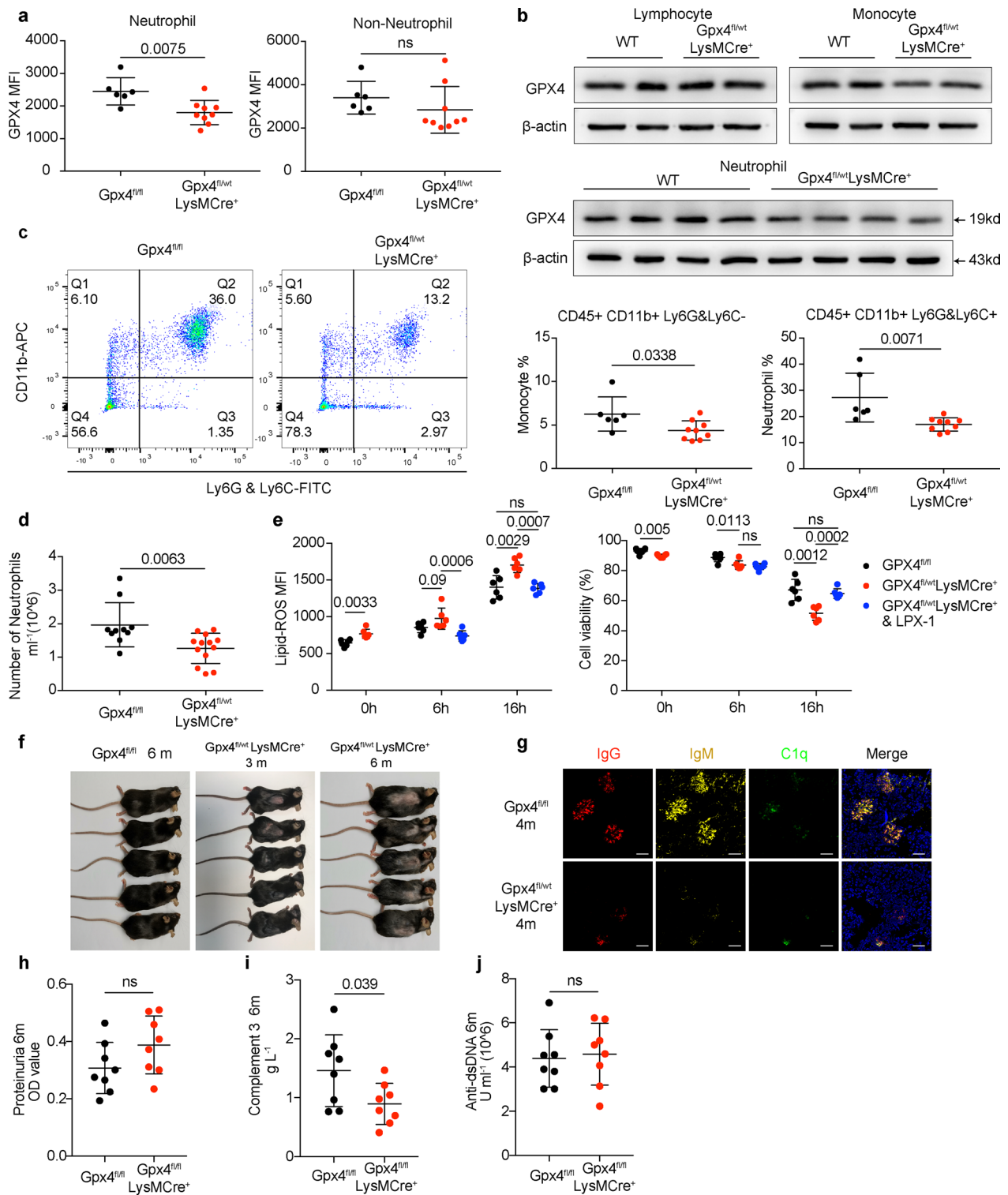
Extended Data Fig. 5 | The expression of cystine transporter SLC7A11 is not different between HC and SLE neutrophils. **a.** Heatmap visualization of RNA-seq analysis on differentially expressed ferroptosis-related genes (Standardized with GAPDH) in neutrophils between new onset treatment-naïve SLE patients (n = 6) and HCs (n = 6). **b.** Western blot validation for SLC7A11 antibody. 293T cells were transfected with *Slc7a11* overexpression plasmid and cells without transfection were used as control. **c.** Western blot assay shows the expression of cystine transporter SLC7A11 in neutrophils from HCs (n = 8) and SLE patients (n = 8). Data are shown as mean \pm SD. ns $p > 0.05$. Two-tailed unpaired Student's t-test was applied.



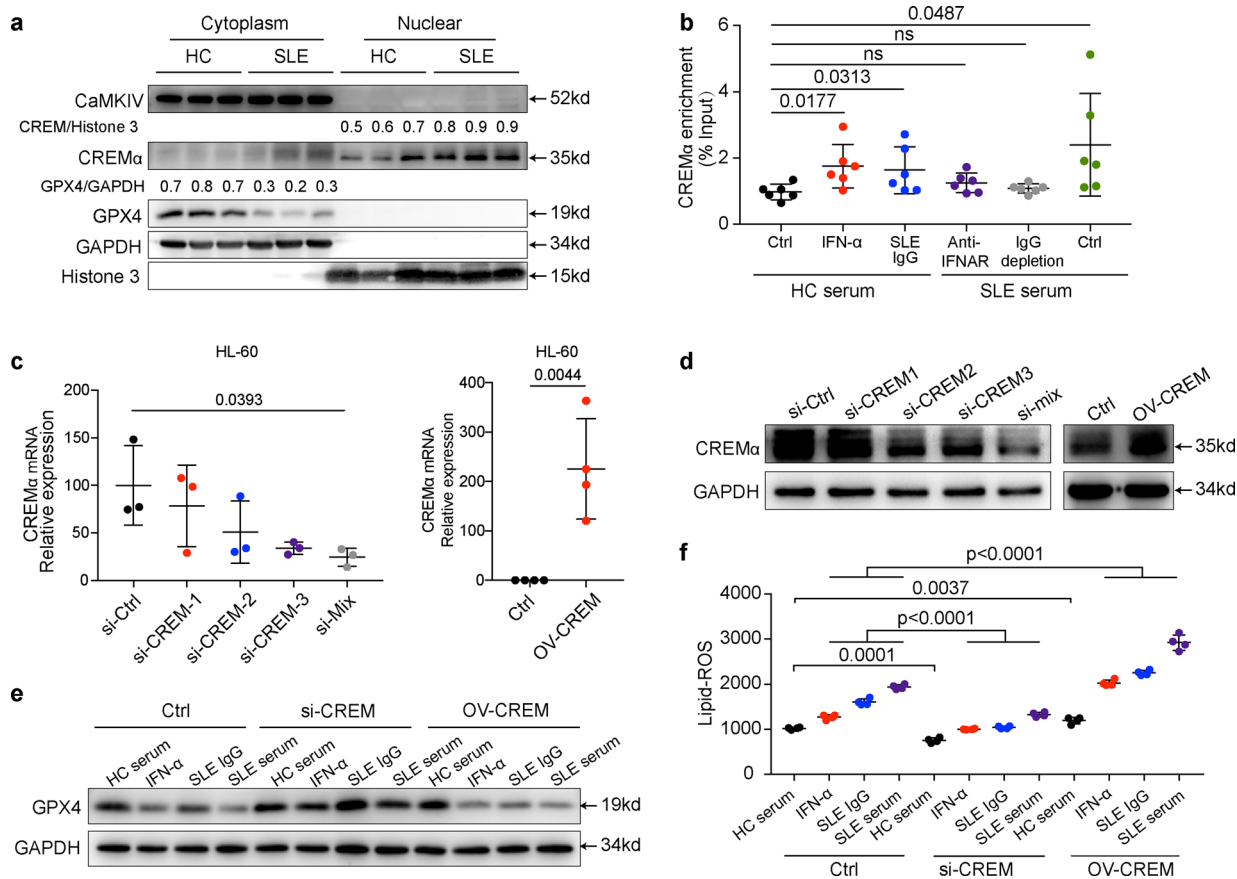
Extended Data Fig. 6 | GPX4 reduction was observed in neutrophils but not other immune cells in SLE. **a**, Flow cytometry quantification of GPX4 expressions in HCs (n=16) and SLE (n=12) neutrophils. **b**, GPX4 expressions in neutrophils from treatment-naïve SLE patients correlated negatively with disease activities as measured by SLEDAI (n=12). **c**, Flow cytometry quantification of GPX4 expressions in lymphocytes (including CD4+ T, CD8+ T, and B cells) and monocytes from HCs (n=11) and SLE patients (n=9). **d-e**, Western blot analysis of GPX4 expressions in lymphocytes and monocytes from HCs (n=11) and SLE patients (n=10). **f-g**, Western blot analysis of GPX4 expression in HC neutrophils, monocytes, and lymphocytes (n=7). **h-i**, Western blot analysis of GPX4 expression in HC neutrophils, monocytes, and lymphocytes (n=7) cultured with 20% HC or SLE serum for 30 hours. **j-k**, Western blot analysis of GPX4 expression in HC neutrophils (n=3) when cultured with 20% HC serum or SLE serum supplemented with CI-amidine (CI, 100 μ M), APX-115 (APX) (pan-NADPH oxidase (NOX) inhibitor, 20 μ M), and GSK2795039 (GSK) (NOX2 inhibitor, 10 μ M). Data are shown as mean \pm SD. ns $p > 0.05$. Two-tailed unpaired Student's t-test was applied.



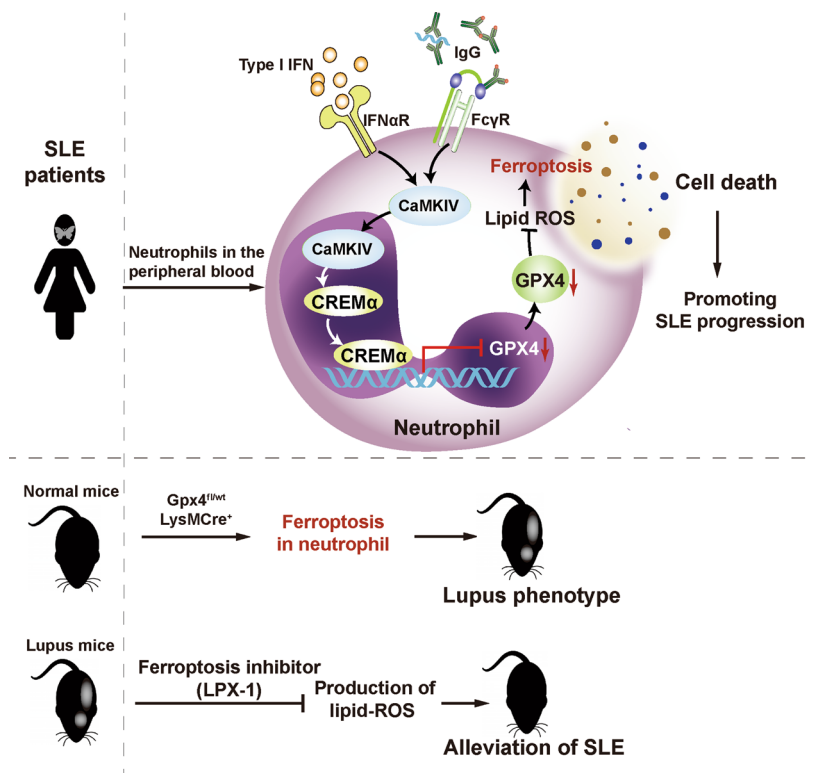
Extended Data Fig. 7 | Fc γ R3 β is essential for the SLE IgG-mediated GPX4 downregulation in neutrophils. **a–b.** Expression correlation analysis between different TLRs or FcRs with GPX4 based on RNA-seq data. In SLE neutrophils, **(a)** TLR signaling pathways are not associated with GPX4 reduction. **(b)** *Fc γ R3 β* but not other FcRs' expression is negatively associated with GPX4 reduction. **c.** Different Fc receptor expressions in HCs ($n=6$) and SLE ($n=6$) analyzed by RNA-seq. **d.** Western blot analysis of Fc γ R3 β expressions in neutrophils, monocytes and lymphocytes from HCs ($n=3$). **e.** GPX4 expressions in HL60 cells after overexpression of Fc γ R3 β ($n=4$). Control referred to cells without transfection. Data are presented as mean \pm SD or median with interquartile range. ns $p > 0.05$. one-tailed or two-tailed unpaired Student's t -test or Mann Whitney test was applied.



Extended Data Fig. 8 | Mice with *Gpx4* haploinsufficiency in neutrophils developed spontaneous lupus-like disease, while *Gpx4*^{fl/fl}*LysMCre*⁺ mice exhibited mild autoimmunity. **a–b.** Flow cytometry quantification and western blot analysis of GPX4 in neutrophils (CD45⁺CD11b⁺Ly6G⁺Ly6C⁺) and non-neutrophils (including monocytes and lymphocytes) from $Gpx4^{fl/fl}$ (n=6) and $Gpx4^{fl/fl}LysMCre^+$ (n=9) mice. **c–d.** Flow cytometry analysis of peripheral neutrophils (CD45⁺CD11b⁺Ly6G⁺Ly6C⁺) and monocytes (CD45⁺CD11b⁺Ly6G⁻Ly6C⁻) from $Gpx4^{fl/fl}$ (c: n=6, d: n=10) and $Gpx4^{fl/fl}LysMCre^+$ (c: n=9, d: n=13) mice. **e.** Flow cytometry quantification of lipid-ROS and cell viability in neutrophils (n=6) from $Gpx4^{fl/fl}LysMCre^+$ mice cultured in complete RPMI 1640 basic medium in the presence or absence of LPX-1 (1 μM). **f.** Skin lesions of $Gpx4^{fl/fl}LysMCre^+$ mice. **g.** Immunofluorescent images of glomeruli in $Gpx4^{fl/fl}$ mice and $Gpx4^{fl/fl}LysMCre^+$ mice. IgG (red), IgM (yellow), C1q (green), and DAPI (blue). **h.** Dot plots show the proteinuria of $Gpx4^{fl/fl}$ and $Gpx4^{fl/fl}LysMCre^+$ mice at 4 months of age assessed by BCA assay. **i.** ELISA assay shows the levels of serum complement 3 in $Gpx4^{fl/fl}$ (n=8) and $Gpx4^{fl/fl}LysMCre^+$ (n=8) mice at 6 months of age. **j.** ELISA assay shows the levels of serum anti-dsDNA antibodies in $Gpx4^{fl/fl}$ (n=8) and $Gpx4^{fl/fl}LysMCre^+$ (n=8) mice at 6 months of age. The scale bar represents 50 μm . Data are shown as mean \pm SD, ns $p > 0.05$. Two-tailed unpaired or paired Student's t-test was applied.



Extended Data Fig. 9 | IFN α and SLE IgG enhanced ferroptosis by promoting binding of CREM to the *Gpx4* promoter. **a**, Western blot analysis of CREM α and CaMKIV in cytoplasm and nucleus of neutrophils from HCs and SLE patients. **b**, Dot plots show the CHIP analysis results on CREM α binding to the promoter of *Gpx4* from neutrophils (n = 6) with indicated treatment: IFN- α (10^5 U ml $^{-1}$), anti-IFNAR ($10 \mu\text{g ml}^{-1}$), SLE IgG (2.4 g L^{-1}) or SLE sera with IgG depletion. **c-d**, Efficiency of CREM α knockdown by siRNA (n = 3) or CREM α over-expression (n = 4) in HL-60 cells validated by qPCR (**c**) and western blot (**d**). **e**, Effect of IFN- α or SLE IgG on GPX4 expressions in HL60 cells after knockdown or overexpression of CREM α . **f**, Efficiency of CREM α knockdown or overexpression on ferroptosis in HL60 cells (n = 4), assessed by flow cytometry using BODIPY C11. Data are shown as mean \pm SD, ns p > 0.05. Two-tailed unpaired or paired Student's t-test was applied.



Extended Data Fig. 10 | The hypothetical model for neutrophil ferroptosis in SLE pathogenesis. Autoantibodies and interferon- α present in SLE sera enhance binding of the transcriptional repressor CREM α to *Gpx4* promoter, which leads to suppressed expression of GPX4 and subsequent elevation of lipid-ROS. These lead to neutrophil ferroptosis and further promote SLE progression in patients. Moreover, mice with neutrophil-specific *Gpx4* haploinsufficiency develop lupus phenotype and inhibition of neutrophil ferroptosis significantly mitigates disease development in lupus-prone mice.

Reporting Summary

Nature Research wishes to improve the reproducibility of the work that we publish. This form provides structure for consistency and transparency in reporting. For further information on Nature Research policies, see our [Editorial Policies](#) and the [Editorial Policy Checklist](#).

Statistics

For all statistical analyses, confirm that the following items are present in the figure legend, table legend, main text, or Methods section.

- | | |
|-----|-----------|
| n/a | Confirmed |
|-----|-----------|
- The exact sample size (n) for each experimental group/condition, given as a discrete number and unit of measurement
 - A statement on whether measurements were taken from distinct samples or whether the same sample was measured repeatedly
 - The statistical test(s) used AND whether they are one- or two-sided
Only common tests should be described solely by name; describe more complex techniques in the Methods section.
 - A description of all covariates tested
 - A description of any assumptions or corrections, such as tests of normality and adjustment for multiple comparisons
 - A full description of the statistical parameters including central tendency (e.g. means) or other basic estimates (e.g. regression coefficient) AND variation (e.g. standard deviation) or associated estimates of uncertainty (e.g. confidence intervals)
 - For null hypothesis testing, the test statistic (e.g. F , t , r) with confidence intervals, effect sizes, degrees of freedom and P value noted
Give P values as exact values whenever suitable.
 - For Bayesian analysis, information on the choice of priors and Markov chain Monte Carlo settings
 - For hierarchical and complex designs, identification of the appropriate level for tests and full reporting of outcomes
 - Estimates of effect sizes (e.g. Cohen's d , Pearson's r), indicating how they were calculated

Our web collection on [statistics for biologists](#) contains articles on many of the points above.

Software and code

Policy information about [availability of computer code](#)

Data collection

BD FACS Aria II (BD, Biosciences, CA, USA) for flow cytometry; TEM-1400 plus electron microscope for Transmission Electron Microscopy; Fluorescence Microscope (ZEISS) for Quantification of NET formation; 7500 Fast Real-Time PCR system (Thermo) for qPCR; A1 HD25/A1R HD25 Nikon confocal laser microscopy (Nikon, Japan) for Immunofluorescence; Illumina Hiseq 4000 platform and StringTie (v1.3.1) for RNA-seq; Western blotting detection system Tanon-5200 (Bio-Tanon, China) for blots and gels; Thermo Scientific Varioskan Flash for ELISA.

Data analysis

GraphPad Prism (version,7.0A) for all statistical analysis; FlowJo (version 10.4, Tree Star); LEGENDplex™ Data Analysis Software (version 8.0); Cuffdiff (v2.1.1); Applied Biosystems 7500 Real-Time PCR Software (v2.3); ImageJ (version 1.50g, NIH); Photoshop CC 2017 (Adobe); Illustrator CC 2017 (Adobe);

For manuscripts utilizing custom algorithms or software that are central to the research but not yet described in published literature, software must be made available to editors and reviewers. We strongly encourage code deposition in a community repository (e.g. GitHub). See the Nature Research [guidelines for submitting code & software](#) for further information.

Data

Policy information about [availability of data](#)

All manuscripts must include a [data availability statement](#). This statement should provide the following information, where applicable:

- Accession codes, unique identifiers, or web links for publicly available datasets
- A list of figures that have associated raw data
- A description of any restrictions on data availability

All raw source data for all experiments included in this study are provided. RNA sequencing data that support the finding of this study have been deposited with the Gene expression Omnibus (GEO) repository under accession number GSE153781. In-house perl scripts were used to analyze RNA-seq data, which are patented

Field-specific reporting

Please select the one below that is the best fit for your research. If you are not sure, read the appropriate sections before making your selection.

- Life sciences
 Behavioural & social sciences
 Ecological, evolutionary & environmental sciences

For a reference copy of the document with all sections, see nature.com/documents/nr-reporting-summary-flat.pdf

Life sciences study design

All studies must disclose on these points even when the disclosure is negative.

Sample size	No statistical methods were used to determine the sample size. Sample sizes were chosen to provide sufficient number of human or mice in each group for informative results and statistical testing, accounting for individual variabilities.
Data exclusions	No data were excluded in our study.
Replication	We have repeated each experiment at least three time to ensure consistent results. All repeats performed showed similar trends.
Randomization	Participant samples and experimental mice were allocated into experimental groups at random. For immunofluorescence, transmission electron microscopy and kidney pathology analysis, the areas were randomly selected.
Blinding	Blinding was not relevant to our study, for the main group of the study population was women of childbearing age

Reporting for specific materials, systems and methods

We require information from authors about some types of materials, experimental systems and methods used in many studies. Here, indicate whether each material, system or method listed is relevant to your study. If you are not sure if a list item applies to your research, read the appropriate section before selecting a response.

Materials & experimental systems

n/a	Involved in the study
<input type="checkbox"/>	<input checked="" type="checkbox"/> Antibodies
<input type="checkbox"/>	<input checked="" type="checkbox"/> Eukaryotic cell lines
<input checked="" type="checkbox"/>	<input type="checkbox"/> Palaeontology and archaeology
<input type="checkbox"/>	<input checked="" type="checkbox"/> Animals and other organisms
<input type="checkbox"/>	<input checked="" type="checkbox"/> Human research participants
<input checked="" type="checkbox"/>	<input type="checkbox"/> Clinical data
<input checked="" type="checkbox"/>	<input type="checkbox"/> Dual use research of concern

Methods

n/a	Involved in the study
<input checked="" type="checkbox"/>	<input type="checkbox"/> ChIP-seq
<input type="checkbox"/>	<input checked="" type="checkbox"/> Flow cytometry
<input checked="" type="checkbox"/>	<input type="checkbox"/> MRI-based neuroimaging

Antibodies

Antibodies used	Anti-glutathione peroxidase 4 (GPX4) antibody (EPNCIR144, ab125066, Abcam; 1:1000), anti-CaMKIV antibody (ab3557, Abcam; 1:1000), anti-histone 3 antibody (ab1791, Abcam; 1:1000), anti-C1q antibody (4.8, ab182451, Abcam, 1:200), anti-neutrophil elastase antibody (ab68672, Abcam, 1:200), anti-CREM antibody (WB: nbp2-16009, NOVUS; 1:1000. CHIP: A5624, Abclonal), anti-GAPDH antibody (10494-1-AP, Proteintech; 1:1000), anti-β-actin (BE0022, Easybio; 1:1000), anti-SLC7A11 antibody (26864-1-AP, Proteintech; 1:1000), anti-histone H3 (citulline R2) antibody (EPR17703, ab176843, Abcam; 1:1000), anti- FcγR3b antibody (MMO272-5L11, ab89207, Abcam; 1:1000), anti-rabbit IgG-HRP (BE0101, Easybio; 1:5000), anti-human IgG-HRP (BE0122, Easybio; 1:5000), anti-mouse IgG-HRP (BE0102, Easybio; 1:5000), PE conjugated anti-mouse Ly-6G (127607, Biolegend; 1:100), PE conjugated anti-human CD16 (561313, BD Pharmingen;1:100), APC conjugated anti-mouse/human CD11b (101212, Biolegend; 1:100), FITC conjugated anti-mouse CD45 (103108, Biolegend; 1:100), FITC conjugated anti-mouse Ly-6G&Ly-6C (553127, BD Pharmingen; 1:100), TruStain FcX anti-CD16/32 (422302, Biolegend; 1:100), goat pAb to mouse IgM Alexa Fluor 647 (ab150123, Abcam; 1:200), goat pAb to rabbit IgG Alexa Fluor 488 (ab150077, Abcam; 1:200), donkey pAb to rabbit IgG Alexa Fluor 647 (ab150075, Abcam; 1:100), goat anti-mouse IgG Alexa Fluor 594 (405326, Biolegend; 1:200), mouse monoclonal antibody against human interferon Alpha/Beta Receptor 1 (MMHAR-3, 21370-3, pbl assay science), anti-CXCL11 antibody (ab9955, Abcam), and anti-human IL-12/23 (ustekinumab) (HY-P9909, Medchem Express).
Validation	All antibodies were obtained commercially validated by the respective company. All antibodies had validation statement provided on the website of the manufacturer. Related technical data sheets can be obtained from the manufacturer’s website using the catalog number provided above.

Eukaryotic cell lines

Policy information about [cell lines](#)

Cell line source(s)	HL-60: KG141, Keygen 293T: CL-0005, Procell
Authentication	The HL-60 cell line was purchased from Library of Chinese Academy of Sciences cells; The 293T cell line was purchased from Procell Corporation. Cell line was authenticated prior to receipt by the commercial vendor using the standard method.
Mycoplasma contamination	Cell line tested negative for mycoplasma contamination
Commonly misidentified lines (See ICLAC register)	The study didn't involve misidentified lines

Animals and other organisms

Policy information about [studies involving animals](#); [ARRIVE guidelines](#) recommended for reporting animal research

Laboratory animals	Female MRL/Mpj and MRL/Mpj-Faslpr (MRL/lpr) mice were used at an age of 12-18 weeks Female Crem-/- C57BL/6 and Camk4-/- C57BL/6 mice were used at an age of 8-20 weeks Female Camk4-/- MRL/lpr mice were used at an age of 18 weeks Female NZB/W F1 mice were used at an age of 12-28 weeks Female and male C57/B6-Gpx4fl/fl (000486, Jackson) and C57/B6-LysMcre (000485, Jackson) mice The GPX4fl/fl mice were bred to the LysMcre mice to generate female and male GPX4fl/wtLysMcre+ and GPX4fl/flLysMcre+ versions of these strains. These mice were used at an age of 12-52 weeks Mice were housed with a dark/light cycle of 12 hours, a temperature of 20-24°C, and a humidity of 45-60%.
Wild animals	The study didn't involve wild animals.
Field-collected samples	The study didn't involve samples collected from the field.
Ethics oversight	All in vivo experiments were performed according to the guidance of the German Animal Welfare Law. Our study was approved by the Institutional Animal Care and Use Committee of Peking Union Medical College Hospital (PUMCH) (JS-1196), Beth Israel Deaconess Medical Center's Institutional Animal Care and Use Committee (088-2015).

Note that full information on the approval of the study protocol must also be provided in the manuscript.

Human research participants

Policy information about [studies involving human research participants](#)

Population characteristics	The characteristics of patients involved in the study were shown in supplementary table1-5,7.
Recruitment	Patients were prospectively recruited in our rheumatology outpatient department fulfilling the diagnosis of SLE. Treated patients involved in the study all received standard medical care to exclude the treatment bias. And sample selection for study inclusion was based on the diagnosis of SLE according to the criteria established by the American College of Rheumatology and therefore no potential self-selection bias is present and hence there is no impact on the results.
Ethics oversight	Informed consent was obtained from all human participants. Our study was approved by the Institutional Review Board of Peking Union Medical College Hospital (PUMCH) (JS-1196) and Beth Israel Deaconess Medical Center's Institutional Review Board (2006P000298).

Note that full information on the approval of the study protocol must also be provided in the manuscript.

Flow Cytometry

Plots

Confirm that:

- The axis labels state the marker and fluorochrome used (e.g. CD4-FITC).
- The axis scales are clearly visible. Include numbers along axes only for bottom left plot of group (a 'group' is an analysis of identical markers).
- All plots are contour plots with outliers or pseudocolor plots.
- A numerical value for number of cells or percentage (with statistics) is provided.

Methodology

Sample preparation	Freshly isolated or cultured neutrophils, lymphocytes and monocytes in different experimental conditions were prepared for flow cytometry analysis.
--------------------	---

Instrument	BD FACS Aria II (BD Biosciences, CA, USA)
Software	FlowJo (version 10.4, Tree Star).
Cell population abundance	The preparation contained greater than 98% neutrophils as confirmed by flow cytometry using CD16 (Biosciences) and CD11b (Biolegend) antibodies.
Gating strategy	According to the parameters of FSC/SSC, cell debris, lymphocyte population, monocyte population, and neutrophil population were distinguished. The neutrophil population had the largest FSC/SSC parameters. Then live cells were identified as 7AAD (-)/Annexin V (-) group. Monocytes and neutrophils were identified as CD45(+)/CD11b(+)/Ly6G&Ly6C(-) and CD45(+)/CD11b(+)/Ly6G&Ly6C(+) respectively in mice.

Tick this box to confirm that a figure exemplifying the gating strategy is provided in the Supplementary Information.